Cite as: T. Xie *et al.*, *Science* 10.1126/science.abc2754 (2020).

Conformational states dynamically populated by a kinase determine its function

Tao Xie, Tamjeed Saleh, Paolo Rossi, Charalampos G. Kalodimos*

Department of Structural Biology, St. Jude Children's Research Hospital, Memphis, TN, USA.

***Corresponding author. Email: babis.kalodimos@stjude.org**

Protein kinases intrinsically sample a number of conformational states with distinct catalytic and binding activities. We used nuclear magnetic resonance spectroscopy to describe in atomic-level detail how Abl kinase interconverts between an active and two discrete inactive structures. Extensive differences in key structural elements among the conformational states give rise to multiple intrinsic regulatory mechanisms. The findings explain how oncogenic mutants can counteract inhibitory mechanisms to constitutively activate the kinase. Energetic dissection revealed the contribution of the activation loop, the DFG motif, the regulatory spine and the gatekeeper residue to kinase regulation. Characterization of the transient conformation to which the drug imatinib binds enabled the elucidation of drug resistance mechanisms. Structural insight into inactive states highlights how they can be leveraged for the design of selective inhibitors.

Protein kinases are key enzymes involved in mediating cell signaling by phosphorylating tyrosine, serine or threonine residues in target proteins. The activity of protein kinases is tightly regulated typically by means of intra-molecular interactions, binding of protein partners, and post-translational modifications (*1*–*3*). Dysregulation of kinase activity by deletions or mutations often results in cancer, inflammation or neurodegeneration (*4*, *5*) and disease-associated kinases are the target of therapeutic intervention by small molecules (*6*, *7*). Many genetic mutations associated with cancer affect kinase domains (*8*).

Evidence from biophysical experiments and computational studies, as well as from structures of kinases in complex with various inhibitors, indicates that protein kinases are dynamic and sample alternate conformational states (*9*–*17*). However, it has proved challenging to monitor these transitions and structurally characterize the manifold of conformational states populated by a kinase. Knowledge of the conformational ensemble could give insight into the mechanisms of regulation. Evolutionary pressure has forced kinases to adopt similar active states so that regions required for catalysis are precisely positioned (*18*, *19*). In contrast, inactive states can be distinct and may in principle vary significantly among kinases. Structural information of the inactive states adopted by kinases could aid in the development of selective inhibitors.

Three key structural elements typically determine whether a kinase adopts the active or an inactive state (*18*, *19*): the catalytic Asp-Phe-Gly (DFG) motif, the activation loop (A-loop), and the αC helix (Fig. 1A). In the fully active state the DFG motif adopts the so-called "DFG-in" state, wherein the Asp (Asp400 in Abl) of DFG points inside the active site cleft and is poised to coordinate Mg-ATP; the A-loop adopts a so-called open conformation that allows substrates to dock onto it to be phosphorylated; and the αC helix adopts the so-called "αC-in" state wherein a conserved αC helix Glu residue (Glu305 in Abl) forms an ion pair with a conserved Lys residue (Lys290 in Abl) in the β3-strand that coordinates the α and β phosphates of the ATP. A significant deviation from this architecture will result in an inactive state.

Abl kinase is involved in a number of signaling pathways that control cell growth, survival, invasion, adhesion and migration (*20*–*22*). The breakpoint cluster region (Bcr)-Abl, an aberrant fusion form of Abl with dysregulated activity causes leukemia and other cancers and is the target of a number of inhibitors, such as imatinib (Gleevec) (*20*, *23*). However, a majority of patients develop mutations that confer resistance to imatinib and other inhibitors (*24*–*28*). While it has been possible to explain how some of these mutations decrease the inhibitor affinity, the mechanistic basis for the effect of mutations in sites remote to the inhibitor is not known. We have used nuclear magnetic resonance (NMR) spectroscopy to structurally characterize how Abl switches between the active and two distinct inactive states and to dissect how the conformational ensemble is exploited by mutants, ligands, post-translational modifications, and inhibitors to regulate the kinase activity and function.

Accessing alternate conformational states of Abl kinase

NMR has provided a wealth of information on the role of dynamics in the regulation of kinases (*14*, *29*–*37*). The ^{1}H-^{15}N– and ^{1}H-^{13}C–correlated NMR spectra of the Abl kinase domain

(hereafter Abl; residues 248-534) labeled in methyl-bearing (Ala, Ile, Met, Leu, Thr and Val) and aromatic residues were of high sensitivity and resolution (fig. S1). In the spectra of unliganded Abl recorded at 20°C or higher, the resonances of the activation loop (A-loop) and nearby residues at the αC helix (Fig. 1A) broaden beyond detection (fig. S1, B and C). Such extreme line broadening is commonly observed in kinases studied by NMR in their unliganded state (*11*, *29*) and has typically prevented a detailed characterization of the A-loop. The A-loop encompasses the DFG motif, forms the docking site for substrate binding, and, in tyrosine kinases, includes the tyrosine residue(s) that are phosphorylated to regulate activity (*38*). We obtained near-complete methyl assignment of Abl by lowering the temperature to 10°C where all of the expected resonances were visible (fig. S1, B and C).

The observed line broadening is due to millisecond timescale conformational transitions indicating the presence of alternate conformational states (*39*). To access the conformational states sampled by Abl, we used the chemical exchange saturation transfer (CEST) NMR technique (*40*, *41*). In this experiment, a weak radiofrequency field is applied to monitor magnetization transfer in sites that undergo conformational exchange. We recorded ^{13}C-based CEST experiments on Abl samples labeled (^{1}H,^{13}C) specifically in the 104 methyl-bearing residues (Fig. 1B and fig. S1A), which afforded high sensitivity even at low temperatures. A CEST profile was obtained for each one of the methyl probes in Abl. If exchange is present (with an exchange rate, k_{ex}, between ~20–500 s^{-1}), a large dip at the chemical shift of the dominant, energetically ground state (G) and a smaller dip at the chemical shift of the alternate, energetically excited state are observed (Fig. 1C and fig. S2). Methyl probes reporting on the conformational transitions are distributed throughout the protein with many of them being located in or near the A-loop and the αC helix (Fig. 1B).

Forty methyl probes (colored cyan in Fig. 1B) showed one minor dip in their CEST profile (e.g., Val318^{CG1} and Ile333^{CD1}; Fig. 1C), while 43 methyl probes (colored magenta in Fig. 1B) showed two minor dips indicating the presence of two distinct energetically excited conformational states (e.g., Leu267^{CD2} and Leu389^{CD2}; Fig. 1C) referred to as E_1 and E_2. CEST data fitting (see Materials and methods) indicated a linear equilibrium, G↔E_1↔E_2 (Fig. 1D). The exchange rate k_{ex} for the G↔E_1 transition is 46.8 ± 4.3 s^{-1} and for the E_1↔E_2 transition is 88.7 ± 13.5 s^{-1}. The population of the ground state (p_G) is 88% whereas the population of either E_1 (p_{E1}) or E_2 (p_{E2}) is 6% indicating that the two excited states are equally stable (Fig. 1D).

Structure of the Abl ground state

The structure of unliganded Abl is not known. We used NMR spectroscopy to determine the structure of the ground state (population 88%; Fig. 1D and fig. S1, B and C) of the isolated Abl kinase domain in solution. The structural data demonstrate that unliganded Abl kinase domain adopts a catalytically active conformation in solution (Fig. 2A and fig. S3, A to C) with the A-loop adopting an open conformation and the DFG motif and αC helix both in the *"in"* state (Fig. 2A). Phe401 of the DFG motif fits snugly into a hydrophobic pocket lined by Val308, Met309, Ile312, Leu317, Val318, and Leu373, and these interactions further stabilize the DFG motif in the "*in*" state. Tyr412, the residue that when phosphorylated stimulates Abl activity (*42*), forms hydrogen bonds through its side chain to Arg381 and Arg405, and these interactions stabilize the open conformation of the A-loop. The phosphate-binding loop (P-loop; also referred to as the Gly-rich loop) is an important region in kinases because it directly affects ligand binding in the active site (*19*, *43*). Tyr272, the bulkiest residue in the P-loop, points inwards and occupies the cleft where the phosphate group of ATP is located (Fig. 2A). Thus, Abl adopts predominantly the active state in solution and inhibitors, such as dasatinib, that selectively target the Abl active state bind with high affinity (fig. S3, D and E) (*44*).

Structure of the Abl excited state 1 (E_1)

To gain structural insight into the low-populated conformational states that Abl samples, we directly measured the ^{13}C chemical shift of the methyls in these two states from the corresponding CEST profiles (Fig. 1C). We next compared the chemical shifts of these two states to the chemical shifts of Abl in complex with twelve different inhibitors (fig. S4). Structural data (*28*, *45–52*) have shown that these inhibitors can capture Abl in distinct conformational states and thus we asked whether any of the low-populated conformational states sampled by unliganded Abl resembles an inhibitor-bound state.

The ^{13}C methyl chemical shifts of the Abl E_1 state showed remarkable similarity to the chemical shifts of Abl in complex with inhibitor PD173955 (Fig. 1E and fig. S5A). To structurally characterize Abl E_1 we sought to increase its population at the expense of the ground state as shown before for other systems (*53–55*). The double amino acid substitution M309L/H415P combined with adjusted pH buffer conditions collectively increased the population of E_1 from 6 to 50% (fig. S5, B to D). NMR data showed that the double amino acid substitution M309L/H415P shifts the equilibrium toward E_1 without eliciting other structural changes (fig. S5, B and E). We used the Abl$^{M309L/H415P}$ variant to obtain NOE-based distance restraints to gain insight into the structure of Abl E_1 (fig. S5, F and G). The structural data showed that Abl in E_1 adopts a structure (Fig. 2B) that is distinct and uncommon among unliganded protein kinases with known structures. Specifically, the DFG motif is flipped 180°, with respect to the active conformation,

and it adopts the DFG-*out* conformation. However, the A-loop remains in an open conformation similar to the active conformation. Because of the DFG flip, the five residues following the DFG motif (Leu403-Met407) of the A-loop are also flipped by 180°. Thus, although the overall structural disposition of the N-terminal part of the A-loop is very similar in the active and in E_1 states, the backbone dihedral angles are very different so that the side chains of the residues point in opposite directions (Fig. 2B). Asp400 is in the "*out*" conformation and swaps positions with Phe401 of the active state. Thus, Asp400 is now located inside a hydrophobic pocket and to compensate for this unfavorable environment its side chain forms a hydrogen bond with the carbonyl oxygen of Val318. With Phe401 flipping inside the ATP-binding pocket, Leu403 swings in the opposite direction. As a result, Arg405, which in the active conformation forms a hydrogen bond with Tyr412 (Fig. 2A), pivots outwards and forms a salt bridge with Glu311 of the αC helix. The αC helix adopts the "*in*" conformation where Glu305 forms an ion pair with Lys290, similarly to the active state (Fig. 2B). Overall, Abl in E_1 adopts the DFG-*out*, αC-helix-*in* conformation and thus it is catalytically inactive. We will refer to E_1 as inactive state 1 (I_1). Structural and NMR data analyses are consistent with Abl in state I_1 adopting a structure that is very similar to the crystal structure of the complex with the PD173955 inhibitor (*46*). Thus, PD173955 binds to and stabilizes a conformational state that already preexists in the conformational ensemble of unliganded Abl (fig. S5H).

Structure of the Abl excited state 2 (E_2)

The ^{13}C methyl chemical shifts of Abl E_2 show an excellent correlation with the chemical shifts of Abl in complex with imatinib (Fig. 1F). The crystal structure of Abl in complex with imatinib showed that a hallmark is the closed conformation of the A-loop (*46*). All of the methyl probes in or around the A-loop experience large chemical shift changes ($\Delta\varpi$) as a result of the A-loop undergoing a large conformational change upon imatinib binding. For example, the two methyl groups of Leu406 have very characteristic chemical shifts; methyl CD1 has a ^{13}C $\Delta\varpi$ of approximately –2.8 p.p.m. and methyl CD2 a ^{13}C $\Delta\varpi$ of approximately 2.1 p.p.m. (Fig. 1F). The excellent correlation of the $\Delta\varpi$ values between E_2 and the imatinib-bound state observed indicates that the A-loop in E_2 adopts the closed conformation. Of note, a number of methyl probes on or nearby the αC helix deviate significantly from linearity (blue spheres in Fig. 1F) suggesting that the αC helix adopts a different conformation in Abl E_2 than that observed in the complex with imatinib.

To gain more detailed structural insight into the Abl E_2 state, we sought to increase its population at the expense of the ground state as we did above for the Abl E_1 state. From the analysis of the crystal structure of the Abl-imatinib complex (*46*), augmented by structural modeling of the unliganded Abl aided by the determined chemical shifts in the E_2 state, we reasoned that the T408Y substitution should stabilize the closed A-loop conformation by forming a hydrogen bond between the hydroxyl of Tyr408 and the side chain of Asp344 or Asn341 (fig. S6A). NMR analysis of the Abl^{T408Y} variant showed that indeed the substitution increases the population of E_2 from 5 to 70% (fig. S6B). Because the exchange between the active and inactive states is slow on the NMR time scale, two sets of peaks are present in the NMR spectra of Abl^{T408Y}: the chemical shifts of one of the sets correspond to those of the ground, active state, while the chemical shifts of the second set correspond to the chemical shifts of the E_2 state as measured by CEST (fig. S6B). The two sets of peaks are connected in a magnetization exchange experiment (fig. S6C) further corroborating that the two states are in dynamic equilibrium. To further increase the population of the E_2 state we produced the M309L/T408Y double substitution (fig. S6D). The NMR data clearly show that the single T408Y or the double M309L/T408Y substitution shift the equilibrium toward E_2 without eliciting other structural changes (fig. S6, B and E). The $Abl^{M309L/T408Y}$ and similar variants (Materials and methods), which have E_2 populated at ~90-100%, allowed us to measure a large number of NOE-based distance restraints (fig. S7A) that were used to determine the structure of the Abl I_2 state (fig. S7B).

The structure of the Abl E_2 state is depicted in Fig. 2C. Compared to the active state, the A-loop in the E_2 state rotates with the middle of the A-loop translating by as much as 35 Å (see arrow in Fig. 2C). A segment in the C terminus of the A-loop folds back and masks the substrate docking site, while Tyr412 occupies the substrate Tyr position thereby preventing substrate binding altogether. Similar to the Abl I_1 state, the DFG motif in Abl E_2 adopts the *"out"* conformation. However, Phe401 of the DFG in the E_2 state does not only flip into the catalytic pocket as was observed in I_1 (Fig. 2B), but in addition it translates by ~11 Å to occupy a hydrophobic pocket that is lined by Leu267, Val275, Ala288, Phe336, and Leu403 (Fig. 2C). This hydrophobic pocket is formed as a result of the void created by Tyr272 (P-loop) swinging outwards and is further stabilized and enlarged by the repositioning of A-loop residues Leu403 and Leu406 (Fig. 2C). The positioning of Phe401 into this hydrophobic pocket directly blocks binding of ATP or competitive inhibitors.

In the E_2 state the entire P-loop undergoes a pronounced rotation and translation with Tyr272, located in the middle of the P-loop, shifting by ~16 Å toward the αC helix (Fig. 2C). The repositioned Tyr272 acts as a wedge to push the αC helix away from the C-lobe. As a result, Glu305 in the αC helix rotates outwards by ~90° and breaks its ion pair with Lys290, an interaction that is required for catalysis (*9*) (Fig. 2C). Thus, the αC helix transitions from the "*in*" conformation in the

active state to the "*out*" conformation in the E_2 state. Taken together, Abl in the E_2 state adopts a fully inactive conformation with the four key structural elements, A-loop, DFG motif, αC helix and P-loop, all being in conformations that are not compatible with either substrate binding or ATP binding or hydrolysis. We will refer to Abl E_2 state as inactive state 2 (I_2).

Structural differences between Abl I_2 and the Abl–imatinib complex

Comparison of the structure of Abl in the I_2 state and the crystal structure of Abl in complex with imatinib (*46*) indicate similarities but also key differences (Fig. 2D). The most important similarity is the conformation of the A-loop that adopts a closed conformation in both the I_2 state and the imatinib complex. Imatinib pushes Phe401 toward the C-lobe by ~3 Å to make room for its pyrimidine ring inside the hydrophobic pocket. The DFG motif is in the "*out*" conformation both in I_2 and the imatinib complex. However, imatinib binding elicits a pronounced change to the structure and disposition of the P-loop and the αC helix. Strong imatinib binding to Abl entails the formation of a hydrogen bond between its secondary amino group and the carboxyl side chain of Glu305 (*46*). This interaction forces the αC helix to the *"in"* conformation. In addition, the P-loop switches from the stretched conformation in I_2 that blocks imatinib from entering into the binding pocket to the kinked conformation observed in the structure of the imatinib complex (Fig. 2D). Thus, imatinib apparently binds selectively to the Abl I_2 state, a low-populated conformational state that resembles the final imatinib complex structure in the A-loop and DFG motif but is very different in the αC helix and P-loop (Fig. 3A). These structural differences explain (fig. S8) the discrepancy between the CEST-derived chemical shifts of certain residues in the Abl I_2 state and their observed chemical shifts in the Abl–imatinib complex (Fig. 1F). Our data suggest that imatinib expends energy to elicit the structural changes required for its binding to Abl likely resulting in a lower affinity. By contrast, the PD173955 inhibitor binds to the I_1 state with minimal structural changes (fig. S5H), which could explain the higher affinity and potency of PD173955 compared to imatinib for Bcr-Abl despite the fewer contacts between the inhibitor and Abl in the PD173955 complex (*46*).

Mechanisms underpinning imatinib-resistance mutations

Imatinib is a selective inhibitor of Abl kinase (*56*, *57*) and is widely used to target Bcr-Abl in chronic myelogenous leukemia (CML) patients (*23*). However, a serious problem is the occurrence of mutations that confer resistance to imatinib in a majority of the patients (*24–27*, *58*). The underlying mechanism of action is straightforward to understand in mutations, e.g., T334I, that occur in positions that line the drug-binding site and sterically clash with imatinib to decrease its affinity for Abl (Fig. 3B). By contrast, the mechanisms conferring drug resistance by mutations in positions remote to the imatinib site have remained enigmatic.

Substitution of His415 by Pro confers resistance to imatinib, despite the fact that this residue is located ~18 Å from the inhibitor (Fig. 3B). We find that Abl^{H415P} binds to imatinib 5-fold weaker than the wild type Abl (Fig. 3C and fig. S9), consistent with a previous report (*59*). To understand the basis for the affinity decrease, we used NMR CEST experiments to measure the effect of the substitution on the Abl conformational ensemble. The data show that H415P destabilizes the Abl I_2 state to the extent that it is not detectable by the CEST experiments, indicating that the population of I_2 in Abl^{H415P} is less than 1% (Fig. 3D). Depletion of the state to which imatinib selectively binds (Fig. 2D), will result in a decrease in imatinib affinity for Abl (Fig. 3C). The destabilization of the I_2 state by the H415P substitution results in the stabilization of the I_1 state, with its population increasing 2-fold (Fig. 3D). The structural basis of these effects can be understood because a Pro residue, given its rigidity and constrained backbone dihedral angles as noted before (*51*), is not compatible with the sharp turn the A-loop makes at this position in the I_2 state, while it can be tolerated in the open conformation of the A-loop observed in Abl I_1 (Fig. 3D).

Several imatinib-resistance mutations cluster in the P-loop, including G269E, Q271H, Y272H and E274V (Fig. 3B). It has been suggested that CML patients with P-loop mutations have a poorer prognosis (*60*). Tyr272 is a key residue in stabilizing the stretched P-loop conformation in the Abl I_2 state by packing against Phe302 of the αC helix and using its hydroxyl group to form a hydrogen bond with the side chain of Glu305 (Fig. 2C). The transition of the P-loop from the kinked conformation observed in the active state to the stretched conformation in the I_2 state is necessary to accommodate the closed conformation of the A-loop in I_2. Quantitative NMR CEST and ^{1}H-^{13}C–correlated experiments show that the Y272H substitution decreases the population of the I_2 state ~7-fold (Fig. 3E), accounting for the ~10-fold decrease in the affinity of imatinib for Abl^{Y272H} (Fig. 3C and fig. S9). His272 is not well poised to form a hydrogen bond with Glu305 and its aromatic π stacking with Phe302 is suboptimal compared to Tyr272, resulting in destabilization of the stretched P-loop conformation and decrease of the Abl I_2 population.

Glu274 forms an ion pair with Lys293, thereby stabilizing the stretched conformation of the P-loop in the I_2 state, is frequently mutated to a Val in patients that have developed imatinib resistance (Fig. 3F). Because the singly mutated Abl^{E274V} variant is not stable enough for CEST studies, we measured the effect of the E274V substitution using the $Abl^{G269E/M309L/T408Y}$ (referred to as Abl^{I2M}) variant, which populates primarily the I_2 state (p_{I2} ~90%), by ^{1}H-^{13}C–correlated

spectra. The data showed that the loss of the Glu274–Lys293 ion pair results in destabilization of the Abl I_2 state by ~1.4 kcal mol^{-1}, which translates to a several fold decrease in its population thus explaining the lower affinity of imatinib for Abl^{E274V} (Fig. 3, C and F).

The F378V imatinib-resistant mutation (Fig. 3B) decreases binding to the inhibitor ~4-fold (Fig. 3C and fig. S9). Consistent with this, NMR analysis of the Abl^{F378V} variant reveals that the F378V substitution decreases the population of the I_2 state ~4-fold (Fig. 3G). On the basis of NMR analysis, we surmise that Val378 exerts its effect by stabilizing the active state, thereby shifting the conformational ensemble toward the active state and depleting the I_2 state (fig. S10A). Our NMR data also explain the imatinib-resistance phenotype of two additional mutations in the P-loop, G269E and Q271H, which exhibit a more complex behavior (fig. S10, B and C). Taken together, our findings illustrate how amino acid substitutions in different structural elements of the Abl kinase can use various mechanisms to destabilize the conformational state to which imatinib selectively binds giving rise to drug resistance.

The role of the regulatory spine in activity regulation

A highly conserved structural feature in protein kinases is the so-called regulatory (also referred to as the hydrophobic) spine (*61*). Mutations in this spine can directly activate or suppress the catalytic activity of kinases (*62*–*64*); however, direct experimental evidence on the underlying mechanisms is lacking. In Abl, the four residues making up the regulatory spine are Met309, Leu320, His380 and Phe401 (Fig. 4A). We used NMR to obtain structural and thermodynamic insight into how mutations in the regulatory spine may remodel the ensemble of the active and the inactive states in Abl. Our data show that the spine is fully assembled in the active state but broken in both the I_1 and I_2 states due to the DFG motif being in the *"out"* conformation (Fig. 4A). The structural deviation is more pronounced in the I_2 state than in the I_1 state because of the move of Phe401 toward the hydrophobic pocket in the nucleotide binding site. ^{13}C CEST and ^{1}H-^{13}C–correlated NMR experiments showed that substitution of Leu, a residue more frequently seen in kinases (*65*), for Met at position 309 increases the population of I_1 and I_2 from 6% each to 10% and ~35%, respectively, and hence increase the total population of inactive states ~4-fold (Fig. 4B). Substitution of the bulkier Ile for Leu at position 320 has an even greater effect with the I_2 state population increasing to 65% (Fig. 4B). The double M309L/L320I substitution switches almost the entire ensemble toward the I_2 state (p_{I2} ~82%) and decreases the active state population to 8%, essentially deactivating the kinase, as confirmed by kinase assays (Fig. 4B and fig. S11). The energetic contribution of the M309L and L320I substitutions toward stabilizing the inactive states is 1.3 and 2.2 kcal mol^{-1}, respectively (Fig. 4C).

Although residues with higher hydrophobicity would be expected to promote the assembly of the spine, and thus stabilize the active state, our data show that this is not the case. Both the Met to Leu (position 309) and the Leu to Ile (position 320) substitutions are toward more hydrophobic residues (*66*) and both stabilize the inactive state. It is likely that in addition to hydrophobicity, the size and shape of the residue side chain at these positions are important in determining the packing and thus the overall assembly of the spine. It is of interest that a Met at the residue corresponding to the Abl 309 position is conserved in ~21% of protein kinases, while a Leu is conserved in ~54% of them. At the residue corresponding to the Abl 320 position, a Leu is conserved in ~54% and an Ile in ~8% of them (*65*). Thus, even conservative mutations that may cause only subtle changes in hydrophobicity and size of the amino acids in the regulatory spine can give rise to pronounced changes in the population of the active and inactive states thereby strongly regulating kinase activity. This finding may explain why the regulatory spine is a hotspot of oncogenic mutations in various kinases (*63*).

Effect of the gatekeeper residue

The residue at the gatekeeper position, which controls accessibility to the hydrophobic region of the ATP pocket in protein kinases, is important for at least two reasons: (i) mutations to bulky residues, such as Ile and Met, at the gatekeeper position (*67*, *68*) stimulate the intrinsic kinase activity and give rise to drastically increased cell transforming and oncogenic activity (*62*, *69*); and (ii) mutations to bulky residues confer drug resistance in some kinases (*24*, *70*). The mechanistic basis for the gatekeeper-induced kinase activation is not known. In Abl, the strongest effect reported is for the gatekeeper Thr334 residue substituted by Ile (*62*, *71*). We characterized Abl^{T334I} by NMR and the analysis showed that the T334I substitution shifts the equilibrium toward the active state. Because the Abl kinase domain already exists predominantly in the active state (p_A ~88%), it is experimentally challenging to quantitate this effect. To do this, we used the Abl^{I2M} variant, which populates primarily the I_2 state (p_{I2} ~90%) while the active state is only marginally stable (p_A ~10%) (Fig. 4D). T334I reverses the populations by strongly promoting the active state (p_A ~93%) (Fig. 4D). The data show that the Ile in the gatekeeper position stabilizes the active state by ~3.2 kcal mol^{-1} (Fig. 4C) and reveal that the basis for kinase activation is a shift of the conformational ensemble toward the catalytically active state. Presumably, the Ile exerts its effect by stabilizing the hydrophobic spine (*65*) through favorable contacts with their nonpolar side chains (Fig. 4D).

The role of the DFG motif in activity regulation

Mutations in the DFG motif have been identified as "drivers"

in human cancers in several kinases (*72*). Although the highly conserved nature of the Asp residue in the DFG motif is explained by its key role in the chemical steps of the catalysis (*73*), the reason for the conservation of the Phe residue is not well understood (*74*). We thus prepared the Abl^{F401V} variant, which NMR data show that it adopts almost exclusively (higher than 95%) the I_2 state (Fig. 4E). The F401V substitution in Abl flips the DFG motif from its preferable *"in"* state to the *"out"* state, which is stabilized by ~3.0 kcal mol^{-1} (Fig. 4C). In agreement, kinase assays showed that the catalytic activity of Abl^{F401V} is at least 20-fold lower than that of the wild-type protein (Fig. 4E and fig. S11). We observed a similarly strong shift toward the DFG-*"out"* state in the Abl^{F401Y} variant (p_{I2} ~90%; Fig. 4E). Thus, even a conservative substitution in this position can affect the ensemble of active and inactive conformational states giving rise to impaired function. This observation is consistent with and may explain findings on other kinases. For example, p38α loses its activity upon substitution of the Phe residue of the DFG motif to Tyr (*75*) and LRRK2, which features a Tyr in this position is retained in an inhibited state and substitution by Phe activates the kinase (*76*). Although Abl I_2 is stabilized in the Abl^{F401V} and Abl^{F401Y} variants, the I_1 state is not. The energetic balance of the contacts of the residue at position 401 with the residues in the two hydrophobic pockets where Phe401 was observed to reside into in the active and the I_2 states (Fig. 2, A and C), will determine the relative populations of the two states and thus the activity of the kinase.

The Phe residue in the DFG motif is conserved in ~90% of kinases, but ~7% of them feature a Leu residue (*65*). In PKA, the Phe to Leu mutation has no effect on its catalytic activity (*65*). The NMR data of Abl^{F401L} show that this variant populates predominantly the active state, similarly to wild type Abl (Fig. 4E) thus explaining why a Leu residue in this position can be tolerated.

The role of A-loop phosphorylation in kinase activation

Phosphorylation of Tyr/Thr/Ser residues in the A-loop is a common mechanism for stimulating the activity of protein kinases (*38*), including Abl (*42*). We quantitated the effect of Abl Tyr412 phosphorylation (pTyr412) on the conformational ensemble of active and inactive states. NMR CEST data show that in Abl^{pY412} both inactive states I_1 and I_2 are depleted and only the active state is detected (Fig. 4F). Our structural data illustrate the mechanistic basis for this effect. Both the active and I_1 states feature an open A-loop conformation with Tyr412 exposed to the solvent. In the active state the phosphate group of pTyr412 forms ion pairs with Arg381 and Arg405 (Fig. 4F). In the I_1 state, although Arg381 is well poised to form a salt bridge with pTyr412, Arg405 is pointing outwards and interacts with Glu311 (Figs. 2B and 4F). Phosphorylation of Tyr412 causes Arg405 to flip inward to form a salt bridge with pTyr412, thereby destabilizing the I_1 state.

In the I_2 state, Tyr412 binds as a pseudosubstrate and blocks the substrate-binding site (Figs. 2C and 4F). The side chain of Tyr412 is positioned in a hydrophobic pocket that is lined by Leu403, L406 and Met407. Thus, phosphorylation of Tyr412 destabilizes the I_2 state by removing the negatively charged pTyr412 from the pocket (Fig. 4F). To quantitatively measure the effect of Tyr412 phosphorylation on the energetics of the ensemble, we used the Abl^{I2M} variant. The population of I_2 in Abl^{I2M} is 90%, whereas it is only 10% in $Abl^{I2M\text{-}pY412}$ (Fig. 4F). Thus, phosphorylation of Tyr412 stabilizes the active state by ~3.0 kcal mol^{-1} (Fig. 4C) and can activate even Abl variants that exist predominantly in the inactive state.

Allosteric regulation of Abl kinase by modulation of the conformational ensemble

Similarly to the Src family kinases (*3*), the docking of the SH3-SH2 regulatory module onto the kinase domain of Abl suppresses its activity (*52*). Because no structural data are available on an SH3-SH2-kinase Abl fragment without an inhibitor bound, the structural changes to the kinase domain elicited by the SH3-SH2 module are not known. We prepared and studied by NMR Abl fragments that encompass the SH3-SH2 module and the kinase domain, which for simplicity we refer to as the full kinase (Abl^{FK}). The presence of the SH3-SH2 module in Abl^{FK} increases the population of the I_2 state ~6-fold, from 6% in the isolated kinase domain to 34% in Abl^{FK} (Fig. 5A). As shown previously (*77*), only ~40% of the molecules in Abl^{FK} are found in the fully assembled state, that is where the SH3-SH2 module is docked onto the back of the kinase, while ~60% of the molecules adopt a disassembled conformation. The allosteric inhibitor GNF5, which was previously shown to promote the assembled conformational state (*32*, *77*), increased the population of the assembled Abl^{FK} state to ~95% (*77*). NMR data on Abl^{FK}-GNF5 indicate that GNF5 binding stabilizes the I_2 state so that its population rises to 95% (Fig. 5A). Thus, our data clearly establish that allosteric stabilization of the I_2 state by the SH3-SH2 module is the structural basis for inhibition in Abl^{FK} (Fig. 5B). The I_1 inactive state is not stabilized by the docking of the SH3-SH2 module. The H415P substitution, which abrogates the I_2 state and promotes the I_1 state in the isolated kinase domain (Fig. 3D), shifts the equilibrium markedly toward the active state in $Abl^{FK\text{-}H415P}$ thereby effectively counteracting the autoinhibitory mechanism (Fig. 5, A and B). This explains the puzzling finding that the H415P substitution stimulates Abl kinase activity (*58*).

Quantitative information on the conformational ensemble of Abl^{FK} provides a tool to assess the effect that various factors, such as the gatekeeper, phosphorylation, and allosteric inhibitors exert on the kinase. As shown above for the isolated Abl kinase domain, the T334I gatekeeper

substitution stimulates Abl activity by shifting the equilibrium toward the active state (Fig. 4, C and D). In Abl^{FK}, the T334I substitution promotes the active state even in the presence of the GNF5 allosteric inhibitor (Fig. 5C). Therefore, this single mutation is capable of activating Abl even when the kinase is held almost entirely in its assembled state (Fig. 5C). This finding is consistent with and explains the observation that the T334I variant markedly stimulates kinase activity even in the myristoylated form of Abl (*62*, *69*). Our data also explain why allosteric inhibitors are not effective against the T334I gatekeeper substitution (*78*, *79*), despite the fact that Ile334 is located away from the allosteric pocket. Our finding that $Abl^{FK\text{-}T334I}$ adopts predominantly the active state is consistent with and accounts for the ~10-fold higher potency of axitinib, which binds selectively to the active state of Abl kinase, in inhibiting Bcr-Abl^{T334I} compared to Bcr-Abl (*48*), as the latter exists predominantly in the I_2 state and is not compatible with axitinib binding (Fig. 5D). Similar to the effect exerted by T334I, phosphorylation of the A-loop at Tyr412 counteracts the strong autoinhibitory mechanism in $Abl^{FK\text{-}GNF5}$ by destabilizing the I_2 state (Fig. 4F) and promoting the active state (Fig. 5, B and E). This finding explains the much lower affinity of imatinib for the phosphorylated (pTyr412) Abl (*80*).

An alternative to the fully assembled, down-regulated state of Abl^{FK} is an experimentally observed conformational state wherein the SH2 domain docks on the top of the N-lobe, thus giving rise to an extended conformation (*77*, *81*–*83*). This structural arrangement is known to stimulate the activity of Abl and has been associated with increased leukemogenic activity (*58*, *82*, *84*). The structural basis for this activity stimulation is not understood. To quantitatively assess the effect, we studied by NMR the $Abl^{FK\Delta SH3\text{-}I2M/T231R}$ variant, which includes the I2M triple mutant that populates predominantly the I_2 state, lacks the SH3 domain, which promotes the assembled conformation, and features the T231R substitution, which is thought to stabilize the interface between the SH2 and the N-lobe (*58*, *77*). The results show that docking of SH2 on the N-lobe of the kinase promotes the active state by a factor of ~4, corresponding to an energetic contribution of ~1.2 kcal mol^{-1} (Fig. 5F). In the context of Abl^{FK}, stabilization of the SH2–N-lobe interface is thus expected to increase the population of the active state from ~35% to ~80% (Fig. 4C). Superposition of the structure of an Abl fragment crystallized in the extended conformation (*83*) with the structure of the Abl I_2 state shows that the surface of the N-lobe in the I_2 state is not compatible with SH2 binding (Fig. 5F). A steric clash between the N-lobe Glu294 and the SH2 His233 and Tyr234 forces the loop connecting the αC helix and β3 strand to retract thereby disrupting the ion pair between Glu274 and Lys293 (Fig. 5F), which is essential for the stabilization of the stretched conformation of the P-loop observed in the Abl I_2 state (Fig. 3F). Taken together, our data show that binding of the SH2 domain on the top of the N-lobe disrupts the αC helix/P-loop conformation in the I_2 state and thus shifts the equilibrium toward the fully active state. Of note, the T231R mutation has been identified as a patient-derived imatinib-resistant variant. Our data explain how the T231R substitution, which strengthens the SH2–N-lobe interface, confers resistance to imatinib (*58*).

pH changes redistribute the populations between the inactive states

Given the distinct environment of Asp400 in the three conformational states (Fig. 6, A to C), we asked whether subtle changes in the electrostatic environment coupled to variations in Asp400 pK_a could affect the conformational ensemble and thus the kinase activity. We measured the populations of the three conformational states of Abl as a function of pH (Fig. 6, D and E) and found that even relatively small changes in the pH can have a substantial effect on the relative stability of the two inactive states. Specifically, although at pH 7.1 the I_1 and I_2 states have the same population, at pH 6.5 the I_1 state is several-fold higher than the I_2 (Fig. 6F). Conversely, at pH 7.7 the I_2 state is much more stable than the I_1 state. Because of the high energy (*85*) required to bury the charged side chain of Asp400 in the hydrophobic pocket in the I_1 state, Asp400 needs to be protonated (*86*). This is in agreement with our observation that lower pH values favor the I_1 state. Of interest, pH changes within this range (6.5-7.7) do not seem to affect the relative stability of the active vs. the inactive states but rather only redistributes the population within the two inactive states.

Activation energy of the DFG transition

The kinetics of the DFG flip determine how fast a kinase is activated or inhibited (*86*, *87*) as it toggles between active and inactive states in response to stimuli. The kinetics of the DFG flip may also determine the rate of ADP release (*74*), which is typically the rate-limiting step in kinase catalysis (*73*). To measure the activation energy of the DFG transition, which governs its kinetics, we measured the exchange rate (k_{ex}) between the active state and the I_1 state as a function of temperature (Fig. 6, G and H). The data showed that the activation energy of the DFG transition from the active to the inactive state is ~36 kcal mol^{-1} (Fig. 6F). This large energy barrier indicates that the DFG flip in Abl kinase entails pronounced structural rearrangement in the transition state and explains why the DFG flip is associated with intrinsically slow kinetics.

Discussion

Here we describe in structural and energetic terms the transition of Abl kinase between its active and two inactive

conformational states. All of these states are intrinsic to the isolated kinase domain and they determine how the kinase responds to regulatory stimuli, substrate and ligand binding, allosteric interactions, and post-translational modifications. Abl kinase populates two distinct inactive states that are quite different from each other. Whereas the DFG motif is in the *"out"* conformation in both I_1 and I_2 states, the A-loop and the αC helix adopt very different conformations. Thus, there are various mechanisms and pathways for a kinase to switch to an inactive conformation.

The Abl I_2 state, which adopts a fully inactive conformation is selectively stabilized in the full-length kinase (Fig. 5B). The biological significance of the I_1 state is not apparent. Although our data suggest that I_1 lies in the pathway between the active and the I_2 state, depletion of the I_1 state has no effect on the population of the I_2 state (Fig. 2E) and therefore is likely not an obligatory intermediate species. Moreover, a single mutation (H415P) that abrogates the I_2 state converts the kinase to its fully active conformation with the I_1 state being very poorly populated even in the full length Abl kinase. That is, the inhibitory mechanism in Abl imposed by the docking of the regulatory module onto the kinase operates only on the I_2 state and not the I_1 state (Fig. 5, A and B). Similarly, mutations in the DFG motif that inhibit the kinase exert their effect by selectively stabilizing the I_2 state and not the I_1 (Fig. 4E). It is possible that the I_1 state is a by-product of the evolutionary process that established the active and the I_2 state, the two functional states. Although conformational states such as the I_1 may not be associated with a known biological function they could be leveraged for the design of selective inhibitors. Characterization of a number of kinases employing the approaches described here could provide evidence of the existence of low-populated inactive conformational states in the kinome.

The discovery and structural insight into the Abl I_2 state as the one to which imatinib selectively binds provides the mechanistic basis for explaining a number of patient-derived imatinib-resistance variants located at sites remote to imatinib. Our data demonstrate that all of these amino acid substitutions confer resistance to imatinib by depleting the population of the I_2 state. The I_2 state can be destabilized by altering the arrangement of any of several structural elements in this state, such as the A-loop, the P-loop and the αC helix, either directly or allosterically (Figs. 4 and 5F and fig. S10). These mutations decrease the affinity not only of imatinib but also of other inhibitors, such as nilotinib, ponatinib and rebastinib (*28*), that also select the Abl I_2 state (fig. S4). The structural data of the Abl I_2 state reported here provides an opportunity for optimizing imatinib analogs for higher affinity.

A question that remains largely unaddressed is how many different inactive conformations intrinsic to kinases are present in the kinome (*18*). This is significant not only for better understanding the variety of mechanisms used by kinases to regulate their activity but also for the design of selective inhibitors. Only a limited number of unliganded kinases have been crystalized in an inactive conformation and only in a fraction of them the intact A-loop, P-loop and αC helix are all visible (*65*). Among kinases with a known structure, the Abl I_1 state is unique. The Abl I_2 state is similar to the structure that the insulin receptor kinase (IRK) adopts in its inactive, non-phosphorylated form (*88*). Superposition of the structures of the Abl I_2 state with that of IRK highlights the striking similarities in the disposition of the A-loop, the DFG motif, the P-loop and the αC helix (fig. S12A). Structural and sequence analysis of the two kinases indicated that the residue at position 408 in Abl (1158 in IRK) may be crucial in stabilizing the closed conformation of the A-loop. The single T408Y substitution in Abl increases the I_2 state population by more than an order of magnitude, from 6% to 70% (fig. S6). IRK has a Tyr in this position (fig. S12A). Four more receptor kinases, TrkA, TrkB, IGF1R and MuSK, adopt a similar structure in their inactive state (fig. S12B). All of them feature a Tyr residue in this position. Conversely, three receptor kinases, FLT3, KIT and FMS, that also adopt a similar structure in their inactive state, do not bear a Tyr in this position; however, all of these three kinases require the presence of the juxtamembrane (JM) domain to stabilize their inactive state (fig. S12B). It should be noted that these receptor tyrosine kinases must adopt an inactive conformation in their resting state (*89*) and thus have evolved to stabilize such a conformation. Taken together, these findings underscore two key observations. First, a structurally similar inactive state among different kinases can be elicited by various mechanisms. For example, Abl accomplishes this by the allosteric action of the regulatory module. Some kinases, such as IRK, feature a crucial Tyr residue in the A-loop that directly stabilizes the inactive state. Other kinases, such as KIT, require the docking of the JM domain against the A-loop. Second, several kinases, both in the receptor and non-receptor tyrosine kinase families, share a structurally similar inactive state. This observation suggests that there might be a limited number of structurally-divergent inactive states intrinsic to kinases (*18*). More structural data on the intrinsic inactive conformations of kinases in the absence of inhibitors are needed to discover the full repertoire of their architecture and the mechanisms used to induce these conformations.

Our findings reveal additional mechanisms, other than allosteric interactions by intra-molecular domains and direct binding of inhibitory proteins, that kinases use to induce their inactive states. The regulatory spine can switch the kinase between its active and inactive states even with conservative changes in the amino acid residues that make up the spine. In Abl, the double substitution M309L/L320I in the

spine switches the kinase from a fully active state (p_A ~90%) to an almost fully inactive state (p_A ~8%) (Fig. 4B). This finding explains why many oncogenic mutations map on the regulatory spine (*63*). Another mechanism for a kinase to stabilize its inactive state is to feature an amino acid other than Phe in the DFG motif (Fig. 4E). Finally, our data highlight and explain how a single mutation at the gatekeeper position can completely neutralize autoinhibitory mechanisms to give rise to a fully activated form of a kinase.

Materials and methods

Expression and preparation of proteins

Abl constructs used in this work were cloned from full-length Abl isoform 1b. The coding sequences were cloned into the pET16b vector for expression as maltose binding protein (MBP)-His_6 fusion proteins including a tobacco etch virus (TEV) protease cleavage site. Various Abl mutants were generated using the QuikChange site-directed mutagenesis kit (Agilent) and their sequences were confirmed by DNA sequencing. The following Abl constructs were prepared: Abl^{FK} (residues 1-534 or 83-534), Abl kinase domain (referred to as Abl; residues 248-534), Abl^{G269E}, Abl^{Q271H}, Abl^{Y272H}, Abl^{M309L}, Abl^{E311K}, Abl^{L320I}, Abl^{T334I}, Abl^{F378V}, Abl^{F401V}, Abl^{F401L}, Abl^{F401Y}, Abl^{T408Y}, Abl^{H415P}, $Abl^{G269E/R405E}$, $Abl^{G269E/M309L}$, $Abl^{Y272H/T408Y}$, $Abl^{M309I/E311K}$, $Abl^{M309L/L320I}$, $Abl^{M309L/F401L}$, $Abl^{M309L/T408Y}$, $Abl^{M309L/H415P}$, $Abl^{E311K/T408Y}$, $Abl^{L320I/T408Y}$, $Abl^{F378V/T408Y}$, $Abl^{L389M/T408Y}$, $Abl^{T408Y/H415P}$, $Abl^{G269E/M309L/T334I}$, $Abl^{M309L/L320I/T334I}$, $Abl^{G269E/M309L/T408Y}$, $Abl^{G269E/E274V/M309L/T408Y}$, $Abl^{FK\text{-}M309L}$, $Abl^{FK\text{-}T334I}$, $Abl^{FK\text{-}T408Y}$, $Abl^{FK\text{-}H415P}$, $Abl^{FK\Delta SH3}$ (residues 138-534), $Abl^{FK\Delta SH3\text{-}T231R}$, and $Abl^{FK\Delta SH3\text{-}T231R/G269E/M309L/T408Y}$. Abl constructs were expressed and purified as described previously (*77*). Unlabeled protein samples were produced in cells grown in Luria-Bertani (LB) medium at 37°C in the presence of ampicillin (100 μg ml^{-1}) to an absorbance at 600 nm (A_{600}) of 0.8. Protein induction was induced by the addition of 0.2 mM isopropyl-β-D-1-thiogalactopyranoside (IPTG) and cells were allowed to grow for 48 hours at 16°C. Cells were harvested at A_{600} ~1.8 and resuspended in lysis buffer (50 mM Tris-HCl, 500 mM NaCl, 1 mM phenylmethylsulfonyl fluoride (PMSF), 5 mM β-mercaptoethanol (BME), pH 8). Cells were disrupted by a high-pressure homogenizer and centrifuged at 50,000 × g. Proteins were purified using Ni Sepharose 6 Fast Flow resin (GE Healthcare), followed by tag removal by TEV protease at 4°C (incubation for 16 hours) and gel filtration using Superdex 75 16/60 or 200 16/60 columns (GE Healthcare). Protein concentration was determined spectrophotometrically at 280 nm using the corresponding extinction coefficient. CrkII was cloned into the pET42a vector, and expression and purification were performed as previously described (*90*). Hck kinase used for Abl Tyr412 phosphorylation was cloned into the pET16b vector and was expressed and purified using a similar protocol to Abl.

Inhibitors

All Abl inhibitors (Selleck Chemicals) used in this study were solubilized in DMSO-D_6 (Cambridge Isotope Laboratories) at a concentration of 10-50 mM and titrated to Abl solutions from these concentrated stocks.

ITC experiments

ITC experiments were performed on MicroCal iTC200 or Auto-iTC200 calorimeters (Malvern Instruments Inc.). ITC titrations for each Abl-inhibitor pair were typically performed at 25°C in 25 mM sodium phosphate buffer (pH 7.1) including 75 mM NaCl and 2.0 mM tris(2-carboxyethyl)phosphine (TCEP). Proteins were purified by size exclusion chromatography using corresponding ITC buffers before use. Concentrations of protein and inhibitors were measured spectrophotometrically and by weight, respectively. Proteins were placed in the cell, while the inhibitors were in the syringe with concentrations in the range 8 to 60 μM and 80 to 650 μM, respectively. The small quantity of DMSO remaining in the inhibitor buffer after the transfer from the stock solution was matched in the protein buffer. All solutions were filtered using membrane filters (pore size, 0.45 μm) and thoroughly degassed. The data were fitted with Origin 7.0 (OriginLab Corporation).

NMR sample preparation

Isotopically labeled samples for NMR studies were prepared by growing the cells in minimal (M9) medium. Cells were typically harvested at A_{600} ~1.2. U-[^{13}C,^{15}N]-labeled samples were prepared for the backbone assignment by supplementing the growing medium with $^{15}NH_4Cl$ (1 g l^{-1}) and $^{13}C_6$-glucose (2 g l^{-1}) (CIL and Isotec). The ^1H–^{13}C methyl-labeled samples were prepared as described (*91*, *92*). For Phe and Tyr selective labeling, 50 mg $l^{-1}$of U-[^2H] ε-^1H,^{13}C-Phe and Tyr were used. NMR samples of Abl variants were typically prepared in 25 mM sodium phosphate buffer (pH 7.1) containing 75 mM NaCl, 3.0 mM BME, in 100% ^2H_2O. The concentration of protein samples ranged from 30 μM to 300 μM. Abl-inhibitor complexes for NMR studies were prepared by mixing the protein at low concentration (~10 μM) with the inhibitor in the NMR buffer followed by concentration via ultrafiltration.

NMR spectroscopy

All NMR experiments were acquired on Bruker 1.1 GHz, 900, 850, 800, 700 and 600 MHz spectrometers equipped with cryogenic probes. Spectra of unliganded Abl were typically collected at 10°C whereas spectra for Abl-inhibitor complexes were collected at 10 or 20°C. All NMR data were processed using NMRPipe (*93*) and analyzed using NMRFAM-Sparky (*94*). Backbone ^1H, ^{15}N, and ^{13}C resonance assignment for Abl variants was achieved using 3D HNCACB, CBCA(CO)NH, HNCA, and HNCO experiments. Sidechain methyl and

aromatic resonances were assigned using 3D-^{13}C,^{15}N-NOESY-HMQC and ^{13}C-HMQC-NOESY-HMQC spectra (*95*) aided by the MAGIC software (*96*).

CEST experiments

$^{13}CHD_2$-CEST experiments (*40*, *97*) were recorded on Bruker 1.1 GHz, 900 and 850 MHz spectrometers at 10°C. Protein samples were prepared in 25 mM sodium phosphate (pH 7.1), 75 mM NaCl, 3.0 mM BME, 100% D_2O. Protein concentration for CEST experiments ranged from 0.15 to 0.3 mM. The labeling scheme for the methyl-bearing residues was as follows: (i) [U-^{2}H; Leu,Val-$^{13}CHD_2$/$^{13}CHD_2$], (ii) [U-^{2}H; Ileδ1-$^{13}CHD_2$], (iii) [U-^{2}H; Met-$^{13}CHD_2$], (iv) [U-^{2}H; Ala-$^{13}CHD_2$], and [U-^{2}H; Thr-$^{13}CH_3$]. A series of 2D spectra in a pseudo-3D mode were recorded with a mixing time (T_{mix}) of 500 ms and a weak B_1 radiofrequency fields of 15 and 25 Hz applied at the ^{13}C dimension in steps of 20-25 Hz. A recycle time of 2.0 s was used in all experiments. Peak intensities were measured using NMRFAM-Sparky (*94*). CEST profiles were made by plotting the intensity ratios with and without the T_{mix} period.

CEST data fitting

CEST data were analyzed using ChemEx (https://github.com/gbouvignies/chemex), which numerically simulates the experiment by solving the Bloch-McConnell equations and minimizes the standard χ^2 equation to get best-fit exchange parameters (*41*, *97*). Errors in peak intensity for the ChemEx input were measured from the background noise of the spectra. Uncertainties in the exchange parameters were estimated by Monte Carlo simulations. Fitting data in a three-state exchange process is typically more challenging. For this reason, we sought to assign the individual minor dips to the corresponding excited state (E_1 and E_2). The strong and opposite dependence of the populations of the two excited states on pH facilitated this assignment, further confirmed by the CEST data on the Abl^{H415P} variant, which eliminates the I_2 state. We first proceeded to fit the CEST data for the Abl^{H415P} variant in which the exchange process is a two-state. Methyls were included in a global fitting to a two-state model of conformational exchange ($A \overset{k_{ex}}{\Leftrightarrow} E_1$) based on the following criteria: 1) no overlap with other peak; 2) minor dip could be discerned in CEST profile; 3) no affect by other local dynamics. The calculated k_{ex} and P_{E1} from fitting were 46.8 ± 4.3 s^{-1} and 12.1 ± 0.5% respectively, with a reduced χ^2 (χ_{red}^2) value of 1.38. Next, we fitted the wild-type Abl CEST data by globally fitting to a three-state exchange model as follows:

$A \overset{k_{ex1}}{\Leftrightarrow} E_1 \overset{k_{ex2}}{\Leftrightarrow} E_2$ model 1

$E_1 \overset{k_{ex1}}{\Leftrightarrow} A \overset{k_{ex2}}{\Leftrightarrow} E_2$ model 2

$A \overset{k_{ex1}}{\Leftrightarrow} E_2 \overset{k_{ex2}}{\Leftrightarrow} E_1$ model 3

The χ_{red}^2 values obtained from models 1, 2, and 3 were 1.15, 1.29, and 1.41, respectively, suggesting model 1 is the most appropriate model to fit the data. The exchange parameters obtained from model 1 were k_{ex1} = 12.3 ± 2.1, k_{ex2} = 145.5 ± 22.6 s^{-1}, p_{E1} = 10.6 ± 1.2%, p_{E2} = 9.6 ± 1.1%, parameters obtained from model 2 were k_{ex1} = 14.7 ± 3.6, k_{ex2} = 18.7 ± 2.7 s^{-1}, p_{E1} = 9.9 ± 1.7%, p_{E2} = 7.0 ± 0.7%, and parameters obtained from model 3 were k_{ex1} = 11.2 ± 2.4, k_{ex2} = 136 ± 23.2 s^{-1}, p_{E1} = 21.2± 4.0%, p_{E2} = 9.2 ± 1.2%. Populations of the excited states larger than ~10% were not consistent with the CEST profiles. Furthermore, we couldn't detect any peaks of the excited states in ^{1}H-^{13}C-correlated spectra of Abl recorded over a period of several days, indicating lower populations. Because of the increased number of fitting parameters in a three-state exchange model data fitting can yield multiple minima. We thus globally fit the data to both model 1 and model 2 by fixing k_{ex1} at 46.8 s^{-1}, as determined by the two-state CEST data fitting on Abl^{H415P}. The χ_{red}^2 values were 1.42 and 1.41 for model 1 and model 2, respectively. The exchange parameters obtained from model 1 were k_{ex1} = 46.8 ± 4.3, k_{ex2} = 88.7 ± 13.5 s^{-1}, p_{E1} = 5.9 ± 0.1%, p_{E2} = 6.1 ± 0.7%, and parameters from model 2 were 46.8 ± 4.3, k_{ex2} = 19.8 ± 2.9 s^{-1}, p_{E1} = 5.4 ± 0.1%, p_{E2} = 6.8 ± 0.7%. Model 1 is in agreement with the population shift observed in Abl^{H415P} in which E_2 is eliminated and the population of E_1 is doubled.

Measurement of the populations of the Abl conformational states

Populations of the active (A) and the two inactive states (I_1 and I_2) in the several Abl variants studied in this work were measured by fitting the CEST data as described above and by integrating the resonances corresponding to each state using ^{1}H-^{13}C–correlated spectra. Because the interconversion of states is slow on the NMR time scale a distinct set of resonances are present in a 2D correlated spectrum provided that its population is higher than ~5%. This latter approach was used for Abl variants that did not remain stable over a period of several days typically needed for recording the CEST data. It was successfully used to measure the populations in Abl^{FK}, which gave very poor CEST data because of low solubility and stability. Two variants were produced and tested for Abl^{FK}, one that encompassed residues 1-534 and the other residues 83-534. Both include the full regulatory module consisting of the SH3-SH2 tandem. Given that both variants gave very similar results, and because of the much higher stability of the 83-534 fragment, the latter one was primarily used. Changes in populations as a result of a mutation were expressed in free energy terms as $\Delta\Delta G = -RT(\ln R_W - \ln R_M)$ in kcal mol^{-1}, where R_W and R_M is the ratio of the populations of the two states in the wild-type and the mutant, respectively.

Structure determination

Structures were calculated from experimental methyl-methyl, methyl-aromatic, aromatic-aromatic, methyl-NH and aromatic-NH NOEs (Table S1). Dihedral angles and hydrogen bond restraints were derived from NOE patterns. Complete NOESY spectra assignment conducted iteratively from sparse restraint sets (*98*) using the automated NOESY cross-peak assignment protocol and dihedral angle dynamics simulated annealing within CYANA 3.98 (*99*). NOE peak assignments were manually curated and refined with several CYANA runs. The lowest target function CYANA-derived structure ensemble was subjected to an all-atom restrained molecular dynamics energy refinement in water bath using CNS (*100*). The active conformation is the predominant (~90%) one populated by Abl in solution and hence its structure was determined using standard approaches. By contrast, I_1 and I_2 are marginally stable with either one a population of 6%. As described in the main text, to structurally characterize these states by NMR we sought to increase their population by amino acid substitutions to shift the equilibrium toward these states without eliciting other structural changes. Because we had determined the chemical shifts of the I_1 and I_2 states by CEST, it was straightforward to assess the effect that the amino acid substitutions had on their structure. The M309L/H415P double substitution was found to markedly stabilize the I_1 state with a population of ~50% (fig. S5). NOESY data were then collected using this sample. Detailed chemical shift analyses showed that the structure of the I_1 state is similar to the one of Abl in complex with the PD173955. Especially in protein parts that are remote to the catalytic site, the A-loop and the αC helix, the two structures were essentially identical. For this reason, we used restraints from the Abl– PD173955 for areas that do not change in Abl I_1, whereas we determined de novo the structure of Abl I_1 in all other using the NMR restraints collected on the $Abl^{M309L/H415P}$ variant. To determine the structure of the Abl I_2 state we followed a similar approach. We initially collected a large number of NOEs on the $Abl^{M309L/T408Y}$ variant, which populates the I_2 state at ~85%. Using the preliminary structural data, we gained more insight into the effect of several other mutants and some of them were observed to further increase the population of the I_2 state, but even more importantly, they exhibited much sharper peaks and were more stable. The $Abl^{G269E/M309L/T408Y}$ variant (also referred to as the I2M variant in the main text) increases the I_2 population to 90% and was amenable to higher resolution NMR characterization.

Abl phosphorylation by Hck

To prepare Abl specifically phosphorylated at the Tyr412 residue we used Hck kinase. 2 μM Hck was auto-phosphorylated in 50 mM Tris buffer (pH 7.5) containing 2 mM ATP, 10 mM $MgCl_2$, 50 mM NaCl, and 3.0 mM BME for 1.5 hours at 22°C. Abl (~5 μM) was incubated with 250 nM of auto-phosphorylated Hck for 14-16 hours at 15°C, followed by extensive dialysis against 50 mM Tris buffer (pH 7.5), 50 mM NaCl, 3.0 mM BME to remove ATP, ADP and $MgCl_2$ and ion exchange purification (Source™ 15Q, GE Healthcare) to separate the phosphorylated Abl from any traces of unphosphorylated protein. Abl phosphorylation was monitored by Western blot analysis with an antibody specific to Abl pTyr412 (2865S, Cell Signaling Technology). Western blot indicated phosphorylation of Abl by Hck led to the phosphorylation of Tyr412 and mass spectrometry and NMR spectra confirmed that samples were homogeneous.

Kinase assays

The kinase assays were conducted in 50 mM Tris (pH 7.5), 0.5 mM $MgCl_2$, 100 mM KCl, and 3.0 mM BME at room temperature with CrkII as substrate. 10 μM CrkII was incubated with 0.2 μM Abl in the reaction buffer, with the addition of ATP to a final concentration of 0.1 mM to initiate the reaction. Reactions were stopped at 0, 30, 60, 120, 180, 300, and 600 s by adding SDS-containing loading buffer. Proteins were resolved in a 4-20% SDS-PAGE gel (Bio-Rad Laboratories) and probed by Western blot with antibody to CrkII pTyr221 (3491S, Cell Signaling Technology). All blots were loaded with SuperSignalTM West Pico Plus Chemiluminescent Substrate (34577, Thermo Scientific), visualized using an Amersham Imager 600 (GE Life Sciences) and quantified with ImageJ. Activity of Abl proteins on CrkII are shown as the n-fold activation above the activity at 0 s for each time point.

REFERENCES AND NOTES

1. M. Huse, J. Kuriyan, The conformational plasticity of protein kinases. *Cell* **109**, 275–282 (2002). doi:10.1016/S0092-8674(02)00741-9 Medline
2. R. Bayliss, T. Haq, S. Yeoh, The Ys and wherefores of protein kinase autoinhibition. *Biochim. Biophys. Acta* **1854**, 1586–1594 (2015). doi:10.1016/j.bbapap.2015.04.025 Medline
3. N. H. Shah, J. F. Amacher, L. M. Nocka, J. Kuriyan, The Src module: An ancient scaffold in the evolution of cytoplasmic tyrosine kinases. *Crit. Rev. Biochem. Mol. Biol.* **53**, 535–563 (2018). doi:10.1080/10409238.2018.1495173 Medline
4. P. Lahiry, A. Torkamani, N. J. Schork, R. A. Hegele, Kinase mutations in human disease: Interpreting genotype-phenotype relationships. *Nat. Rev. Genet.* **11**, 60–74 (2010). doi:10.1038/nrg2707 Medline
5. E. D. Fleuren, L. Zhang, J. Wu, R. J. Daly, The kinome 'at large' in cancer. *Nat. Rev. Cancer* **16**, 83–98 (2016). doi:10.1038/nrc.2015.18 Medline
6. J. Zhang, P. L. Yang, N. S. Gray, Targeting cancer with small molecule kinase inhibitors. *Nat. Rev. Cancer* **9**, 28–39 (2009). doi:10.1038/nrc2559 Medline
7. S. Müller, A. Chaikuad, N. S. Gray, S. Knapp, The ins and outs of selective kinase inhibitor development. *Nat. Chem. Biol.* **11**, 818–821 (2015). doi:10.1038/nchembio.1938 Medline
8. P. A. Futreal, L. Coin, M. Marshall, T. Down, T. Hubbard, R. Wooster, N. Rahman, M. R. Stratton, A census of human cancer genes. *Nat. Rev. Cancer* **4**, 177–183 (2004). doi:10.1038/nrc1299 Medline
9. S. S. Taylor, A. P. Kornev, Protein kinases: Evolution of dynamic regulatory proteins. *Trends Biochem. Sci.* **36**, 65–77 (2011). doi:10.1016/j.tibs.2010.09.006 Medline
10. M. Tong, M. A. Seeliger, Targeting conformational plasticity of protein kinases. *ACS Chem. Biol.* **10**, 190–200 (2015). doi:10.1021/cb500870a Medline
11. Y. Xiao, J. C. Liddle, A. Pardi, N. G. Ahn, Dynamics of protein kinases: Insights from

nuclear magnetic resonance. *Acc. Chem. Res.* **48**, 1106–1114 (2015). doi:10.1021/acs.accounts.5b00001 Medline
12. S. Cyphers, E. F. Ruff, J. M. Behr, J. D. Chodera, N. M. Levinson, A water-mediated allosteric network governs activation of Aurora kinase A. *Nat. Chem. Biol.* **13**, 402–408 (2017). doi:10.1038/nchembio.2296 Medline
13. J. A. H. Gilburt, H. Sarkar, P. Sheldrake, J. Blagg, L. Ying, C. A. Dodson, Dynamic equilibrium of the Aurora A kinase activation loop revealed by single-molecule spectroscopy. *Angew. Chem. Int. Ed.* **56**, 11409–11414 (2017). doi:10.1002/anie.201704654 Medline
14. J. Kim, L. G. Ahuja, F. A. Chao, Y. Xia, C. L. McClendon, A. P. Kornev, S. S. Taylor, G. Veglia, A dynamic hydrophobic core orchestrates allostery in protein kinases. *Sci. Adv.* **3**, e1600663 (2017). doi:10.1126/sciadv.1600663 Medline
15. Y. Meng, C. Gao, D. K. Clawson, S. Atwell, M. Russell, M. Vieth, B. Roux, Predicting the conformational variability of Abl tyrosine kinase using molecular dynamics simulations and Markov state models. *J. Chem. Theory Comput.* **14**, 2721–2732 (2018). doi:10.1021/acs.jctc.7b01170 Medline
16. P. M. Ung, R. Rahman, A. Schlessinger, Redefining the protein kinase conformational space with machine learning. *Cell Chem. Biol.* **25**, 916–924.e2 (2018). doi:10.1016/j.chembiol.2018.05.002 Medline
17. N. M. Levinson, O. Kuchment, K. Shen, M. A. Young, M. Koldobskiy, M. Karplus, P. A. Cole, J. Kuriyan, A Src-like inactive conformation in the Abl tyrosine kinase domain. *PLOS Biol.* **4**, e144 (2006). doi:10.1371/journal.pbio.0040144 Medline
18. N. Jura, X. Zhang, N. F. Endres, M. A. Seeliger, T. Schindler, J. Kuriyan, Catalytic control in the EGF receptor and its connection to general kinase regulatory mechanisms. *Mol. Cell* **42**, 9–22 (2011). doi:10.1016/j.molcel.2011.03.004 Medline
19. S. S. Taylor, H. S. Meharena, A. P. Kornev, Evolution of a dynamic molecular switch. *IUBMB Life* **71**, 672–684 (2019). doi:10.1002/iub.2059 Medline
20. J. Colicelli, ABL tyrosine kinases: Evolution of function, regulation, and specificity. *Sci. Signal.* **3**, re6 (2010). doi:10.1126/scisignal.3139re6 Medline
21. E. K. Greuber, P. Smith-Pearson, J. Wang, A. M. Pendergast, Role of ABL family kinases in cancer: From leukaemia to solid tumours. *Nat. Rev. Cancer* **13**, 559–571 (2013). doi:10.1038/nrc3563 Medline
22. S. Panjarian, R. E. Iacob, S. Chen, J. R. Engen, T. E. Smithgall, Structure and dynamic regulation of Abl kinases. *J. Biol. Chem.* **288**, 5443–5450 (2013). doi:10.1074/jbc.R112.438382 Medline
23. B. J. Druker, F. Guilhot, S. G. O'Brien, I. Gathmann, H. Kantarjian, N. Gattermann, M. W. N. Deininger, R. T. Silver, J. M. Goldman, R. M. Stone, F. Cervantes, A. Hochhaus, B. L. Powell, J. L. Gabrilove, P. Rousselot, J. Reiffers, J. J. Cornelissen, T. Hughes, H. Agis, T. Fischer, G. Verhoef, J. Shepherd, G. Saglio, A. Gratwohl, J. L. Nielsen, J. P. Radich, B. Simonsson, K. Taylor, M. Baccarani, C. So, L. Letvak, R. A. Larson; IRIS Investigators, Five-year follow-up of patients receiving imatinib for chronic myeloid leukemia. *N. Engl. J. Med.* **355**, 2408–2417 (2006). doi:10.1056/NEJMoa062867 Medline
24. M. E. Gorre, M. Mohammed, K. Ellwood, N. Hsu, R. Paquette, P. N. Rao, C. L. Sawyers, Clinical resistance to STI-571 cancer therapy caused by BCR-ABL gene mutation or amplification. *Science* **293**, 876–880 (2001). doi:10.1126/science.1062538 Medline
25. S. Roumiantsev, N. P. Shah, M. E. Gorre, J. Nicoll, B. B. Brasher, C. L. Sawyers, R. A. Van Etten, Clinical resistance to the kinase inhibitor STI-571 in chronic myeloid leukemia by mutation of Tyr-253 in the Abl kinase domain P-loop. *Proc. Natl. Acad. Sci. U.S.A.* **99**, 10700–10705 (2002). doi:10.1073/pnas.162140299 Medline
26. N. P. Shah, J. M. Nicoll, B. Nagar, M. E. Gorre, R. L. Paquette, J. Kuriyan, C. L. Sawyers, Multiple BCR-ABL kinase domain mutations confer polyclonal resistance to the tyrosine kinase inhibitor imatinib (STI571) in chronic phase and blast crisis chronic myeloid leukemia. *Cancer Cell* **2**, 117–125 (2002). doi:10.1016/S1535-6108(02)00096-X Medline
27. M. Azam, R. R. Latek, G. Q. Daley, Mechanisms of autoinhibition and STI-571/imatinib resistance revealed by mutagenesis of BCR-ABL. *Cell* **112**, 831–843 (2003). doi:10.1016/S0092-8674(03)00190-9 Medline
28. W. W. Chan, S. C. Wise, M. D. Kaufman, Y. M. Ahn, C. L. Ensinger, T. Haack, M. M. Hood, J. Jones, J. W. Lord, W. P. Lu, D. Miller, W. C. Patt, B. D. Smith, P. A. Petillo, T. J. Rutkoski, H. Telikepalli, L. Vogeti, T. Yao, L. Chun, R. Clark, P. Evangelista, L. C. Gavrilescu, K. Lazarides, V. M. Zaleskas, L. J. Stewart, R. A. Van Etten, D. L. Flynn, Conformational control inhibition of the BCR-ABL1 tyrosine kinase, including the gatekeeper T315I mutant, by the switch-control inhibitor DCC-2036. *Cancer Cell* **19**, 556–568 (2011). doi:10.1016/j.ccr.2011.03.003 Medline
29. S. Wiesner, L. E. Wybenga-Groot, N. Warner, H. Lin, T. Pawson, J. D. Forman-Kay, F. Sicheri, A change in conformational dynamics underlies the activation of Eph receptor tyrosine kinases. *EMBO J.* **25**, 4686–4696 (2006). doi:10.1038/sj.emboj.7601315 Medline
30. N. Amatya, T. E. Wales, A. Kwon, W. Yeung, R. E. Joseph, D. B. Fulton, N. Kannan, J. R. Engen, A. H. Andreotti, Lipid-targeting pleckstrin homology domain turns its autoinhibitory face toward the TEC kinases. *Proc. Natl. Acad. Sci. U.S.A.* **116**, 21539–21544 (2019). doi:10.1073/pnas.1907566116 Medline
31. Y. Xiao, T. Lee, M. P. Latham, L. R. Warner, A. Tanimoto, A. Pardi, N. G. Ahn, Phosphorylation releases constraints to domain motion in ERK2. *Proc. Natl. Acad. Sci. U.S.A.* **111**, 2506–2511 (2014). doi:10.1073/pnas.1318899111 Medline
32. L. Skora, J. Mestan, D. Fabbro, W. Jahnke, S. Grzesiek, NMR reveals the allosteric opening and closing of Abelson tyrosine kinase by ATP-site and myristoyl pocket inhibitors. *Proc. Natl. Acad. Sci. U.S.A.* **110**, E4437–E4445 (2013). doi:10.1073/pnas.1314712110 Medline
33. Y. Tokunaga, K. Takeuchi, H. Takahashi, I. Shimada, Allosteric enhancement of MAP kinase p38α's activity and substrate selectivity by docking interactions. *Nat. Struct. Mol. Biol.* **21**, 704–711 (2014). doi:10.1038/nsmb.2861 Medline
34. P. C. Aoto, B. T. Martin, P. E. Wright, NMR characterization of information flow and allosteric communities in the MAP kinase p38γ. *Sci. Rep.* **6**, 28655 (2016). doi:10.1038/srep28655 Medline
35. H. Chen, W. M. Marsiglia, M. K. Cho, Z. Huang, J. Deng, S. P. Blais, W. Gai, S. Bhattacharya, T. A. Neubert, N. J. Traaseth, M. Mohammadi, Elucidation of a four-site allosteric network in fibroblast growth factor receptor tyrosine kinases. *eLife* **6**, e21137 (2017). doi:10.7554/eLife.21137 Medline
36. A. Piserchio, M. Warthaka, T. S. Kaoud, K. Callaway, K. N. Dalby, R. Ghose, Local destabilization, rigid body, and fuzzy docking facilitate the phosphorylation of the transcription factor Ets-1 by the mitogen-activated protein kinase ERK2. *Proc. Natl. Acad. Sci. U.S.A.* **114**, E6287–E6296 (2017). doi:10.1073/pnas.1702973114 Medline
37. G. S. Kumar, M. W. Clarkson, M. B. A. Kunze, D. Granata, A. J. Wand, K. Lindorff-Larsen, R. Page, W. Peti, Dynamic activation and regulation of the mitogen-activated protein kinase p38. *Proc. Natl. Acad. Sci. U.S.A.* **115**, 4655–4660 (2018). doi:10.1073/pnas.1721441115 Medline
38. B. Nolen, S. Taylor, G. Ghosh, Regulation of protein kinases; controlling activity through activation segment conformation. *Mol. Cell* **15**, 661–675 (2004). doi:10.1016/j.molcel.2004.08.024 Medline
39. T. R. Alderson, L. E. Kay, Unveiling invisible protein states with NMR spectroscopy. *Curr. Opin. Struct. Biol.* **60**, 39–49 (2020). doi:10.1016/j.sbi.2019.10.008 Medline
40. E. Rennella, R. Huang, A. Velyvis, L. E. Kay, $^{13}CHD_2$-CEST NMR spectroscopy provides an avenue for studies of conformational exchange in high molecular weight proteins. *J. Biomol. NMR* **63**, 187–199 (2015). doi:10.1007/s10858-015-9974-z Medline
41. P. Vallurupalli, A. Sekhar, T. Yuwen, L. E. Kay, Probing conformational dynamics in biomolecules via chemical exchange saturation transfer: A primer. *J. Biomol. NMR* **67**, 243–271 (2017). doi:10.1007/s10858-017-0099-4 Medline
42. B. B. Brasher, R. A. Van Etten, c-Abl has high intrinsic tyrosine kinase activity that is stimulated by mutation of the Src homology 3 domain and by autophosphorylation at two distinct regulatory tyrosines. *J. Biol. Chem.* **275**, 35631–35637 (2000). doi:10.1074/jbc.M005401200 Medline
43. M. A. Seeliger, P. Ranjitkar, C. Kasap, Y. Shan, D. E. Shaw, N. P. Shah, J. Kuriyan, D. J. Maly, Equally potent inhibition of c-Src and Abl by compounds that recognize inactive kinase conformations. *Cancer Res.* **69**, 2384–2392 (2009). doi:10.1158/0008-5472.CAN-08-3953 Medline
44. N. Vajpai, A. Strauss, G. Fendrich, S. W. Cowan-Jacob, P. W. Manley, S. Grzesiek, W. Jahnke, Solution conformations and dynamics of ABL kinase-inhibitor complexes determined by NMR substantiate the different binding modes of imatinib/nilotinib and dasatinib. *J. Biol. Chem.* **283**, 18292–18302 (2008). doi:10.1074/jbc.M801337200 Medline
45. J. S. Tokarski, J. A. Newitt, C. Y. J. Chang, J. D. Cheng, M. Wittekind, S. E. Kiefer, K. Kish, F. Y. F. Lee, R. Borzillerri, L. J. Lombardo, D. Xie, Y. Zhang, H. E. Klei, The structure of Dasatinib (BMS-354825) bound to activated ABL kinase domain elucidates its inhibitory activity against imatinib-resistant ABL mutants. *Cancer*

Res. **66**, 5790–5797 (2006). doi:10.1158/0008-5472.CAN-05-4187 Medline
46. B. Nagar, W. G. Bornmann, P. Pellicena, T. Schindler, D. R. Veach, W. T. Miller, B. Clarkson, J. Kuriyan, Crystal structures of the kinase domain of c-Abl in complex with the small molecule inhibitors PD173955 and imatinib (STI-571). *Cancer Res.* **62**, 4236–4243 (2002). Medline
47. N. M. Levinson, S. G. Boxer, Structural and spectroscopic analysis of the kinase inhibitor bosutinib and an isomer of bosutinib binding to the Abl tyrosine kinase domain. *PLOS ONE* **7**, e29828 (2012). doi:10.1371/journal.pone.0029828 Medline
48. T. Pemovska, E. Johnson, M. Kontro, G. A. Repasky, J. Chen, P. Wells, C. N. Cronin, M. McTigue, O. Kallioniemi, K. Porkka, B. W. Murray, K. Wennerberg, Axitinib effectively inhibits BCR-ABL1(T315I) with a distinct binding conformation. *Nature* **519**, 102–105 (2015). doi:10.1038/nature14119 Medline
49. E. Weisberg, P. W. Manley, W. Breitenstein, J. Brüggen, S. W. Cowan-Jacob, A. Ray, B. Huntly, D. Fabbro, G. Fendrich, E. Hall-Meyers, A. L. Kung, J. Mestan, G. Q. Daley, L. Callahan, L. Catley, C. Cavazza, M. Azam, D. Neuberg, R. D. Wright, D. G. Gilliland, J. D. Griffin, Characterization of AMN107, a selective inhibitor of native and mutant Bcr-Abl. *Cancer Cell* **7**, 129–141 (2005). doi:10.1016/j.ccr.2005.01.007 Medline
50. T. Zhou, L. Commodore, W.-S. Huang, Y. Wang, M. Thomas, J. Keats, Q. Xu, V. M. Rivera, W. C. Shakespeare, T. Clackson, D. C. Dalgarno, X. Zhu, Structural mechanism of the Pan-BCR-ABL inhibitor ponatinib (AP24534): Lessons for overcoming kinase inhibitor resistance. *Chem. Biol. Drug Des.* **77**, 1–11 (2011). doi:10.1111/j.1747-0285.2010.01054.x Medline
51. M. A. Young, N. P. Shah, L. H. Chao, M. Seeliger, Z. V. Milanov, W. H. Biggs III, D. K. Treiber, H. K. Patel, P. P. Zarrinkar, D. J. Lockhart, C. L. Sawyers, J. Kuriyan, Structure of the kinase domain of an imatinib-resistant Abl mutant in complex with the Aurora kinase inhibitor VX-680. *Cancer Res.* **66**, 1007–1014 (2006). doi:10.1158/0008-5472.CAN-05-2788 Medline
52. B. Nagar, O. Hantschel, M. A. Young, K. Scheffzek, D. Veach, W. Bornmann, B. Clarkson, G. Superti-Furga, J. Kuriyan, Structural basis for the autoinhibition of c-Abl tyrosine kinase. *Cell* **112**, 859–871 (2003). doi:10.1016/S0092-8674(03)00194-6 Medline
53. G. Bouvignies, P. Vallurupalli, D. F. Hansen, B. E. Correia, O. Lange, A. Bah, R. M. Vernon, F. W. Dahlquist, D. Baker, L. E. Kay, Solution structure of a minor and transiently formed state of a T4 lysozyme mutant. *Nature* **477**, 111–114 (2011). doi:10.1038/nature10349 Medline
54. L. Chen, V. Balabanidou, D. P. Remeta, C. A. Minetti, A. G. Portaliou, A. Economou, C. G. Kalodimos, Structural instability tuning as a regulatory mechanism in protein-protein interactions. *Mol. Cell* **44**, 734–744 (2011). doi:10.1016/j.molcel.2011.09.022 Medline
55. S. R. Tzeng, C. G. Kalodimos, Allosteric inhibition through suppression of transient conformational states. *Nat. Chem. Biol.* **9**, 462–465 (2013). doi:10.1038/nchembio.1250 Medline
56. Y.-L. Lin, Y. Meng, W. Jiang, B. Roux, Explaining why Gleevec is a specific and potent inhibitor of Abl kinase. *Proc. Natl. Acad. Sci. U.S.A.* **110**, 1664–1669 (2013). doi:10.1073/pnas.1214330110 Medline
57. C. Wilson, R. V. Agafonov, M. Hoemberger, S. Kutter, A. Zorba, J. Halpin, V. Buosi, R. Otten, D. Waterman, D. L. Theobald, D. Kern, Using ancient protein kinases to unravel a modern cancer drug's mechanism. *Science* **347**, 882–886 (2015). doi:10.1126/science.aaa1823 Medline
58. D. W. Sherbenou, O. Hantschel, I. Kaupe, S. Willis, T. Bumm, L. P. Turaga, T. Lange, K.-H. Dao, R. D. Press, B. J. Druker, G. Superti-Furga, M. W. Deininger, BCR-ABL SH3-SH2 domain mutations in chronic myeloid leukemia patients on imatinib. *Blood* **116**, 3278–3285 (2010). doi:10.1182/blood-2008-10-183665 Medline
59. M. I. Davis, J. P. Hunt, S. Herrgard, P. Ciceri, L. M. Wodicka, G. Pallares, M. Hocker, D. K. Treiber, P. P. Zarrinkar, Comprehensive analysis of kinase inhibitor selectivity. *Nat. Biotechnol.* **29**, 1046–1051 (2011). doi:10.1038/nbt.1990 Medline
60. S. Branford, Z. Rudzki, S. Walsh, I. Parkinson, A. Grigg, J. Szer, K. Taylor, R. Herrmann, J. F. Seymour, C. Arthur, D. Joske, K. Lynch, T. Hughes, Detection of BCR-ABL mutations in patients with CML treated with imatinib is virtually always accompanied by clinical resistance, and mutations in the ATP phosphate-binding loop (P-loop) are associated with a poor prognosis. *Blood* **102**, 276–283 (2003). doi:10.1182/blood-2002-09-2896 Medline
61. A. P. Kornev, S. S. Taylor, L. F. Ten Eyck, A helix scaffold for the assembly of active protein kinases. *Proc. Natl. Acad. Sci. U.S.A.* **105**, 14377–14382 (2008). doi:10.1073/pnas.0807988105 Medline
62. M. Azam, M. A. Seeliger, N. S. Gray, J. Kuriyan, G. Q. Daley, Activation of tyrosine kinases by mutation of the gatekeeper threonine. *Nat. Struct. Mol. Biol.* **15**, 1109–1118 (2008). doi:10.1038/nsmb.1486 Medline
63. J. Hu, L. G. Ahuja, H. S. Meharena, N. Kannan, A. P. Kornev, S. S. Taylor, A. S. Shaw, Kinase regulation by hydrophobic spine assembly in cancer. *Mol. Cell. Biol.* **35**, 264–276 (2015). doi:10.1128/MCB.00943-14 Medline
64. A. P. Kornev, S. S. Taylor, Dynamics-driven allostery in protein kinases. *Trends Biochem. Sci.* **40**, 628–647 (2015). doi:10.1016/j.tibs.2015.09.002 Medline
65. H. S. Meharena, P. Chang, M. M. Keshwani, K. Oruganty, A. K. Nene, N. Kannan, S. S. Taylor, A. P. Kornev, Deciphering the structural basis of eukaryotic protein kinase regulation. *PLOS Biol.* **11**, e1001680 (2013). doi:10.1371/journal.pbio.1001680 Medline
66. J. Kyte, R. F. Doolittle, A simple method for displaying the hydropathic character of a protein. *J. Mol. Biol.* **157**, 105–132 (1982). doi:10.1016/0022-2836(82)90515-0 Medline
67. A. C. Bishop, J. A. Ubersax, D. T. Petsch, D. P. Matheos, N. S. Gray, J. Blethrow, E. Shimizu, J. Z. Tsien, P. G. Schultz, M. D. Rose, J. L. Wood, D. O. Morgan, K. M. Shokat, A chemical switch for inhibitor-sensitive alleles of any protein kinase. *Nature* **407**, 395–401 (2000). doi:10.1038/35030148 Medline
68. S. B. Hari, E. A. Merritt, D. J. Maly, Sequence determinants of a specific inactive protein kinase conformation. *Chem. Biol.* **20**, 806–815 (2013). doi:10.1016/j.chembiol.2013.05.005 Medline
69. R. E. Iacob, T. Pene-Dumitrescu, J. Zhang, N. S. Gray, T. E. Smithgall, J. R. Engen, Conformational disturbance in Abl kinase upon mutation and deregulation. *Proc. Natl. Acad. Sci. U.S.A.* **106**, 1386–1391 (2009). doi:10.1073/pnas.0811912106 Medline
70. D. W. Bell, I. Gore, R. A. Okimoto, N. Godin-Heymann, R. Sordella, R. Mulloy, S. V. Sharma, B. W. Brannigan, G. Mohapatra, J. Settleman, D. A. Haber, Inherited susceptibility to lung cancer may be associated with the T790M drug resistance mutation in EGFR. *Nat. Genet.* **37**, 1315–1316 (2005). doi:10.1038/ng1671 Medline
71. B. J. Lee, N. P. Shah, Identification and characterization of activating ABL1 1b kinase mutations: Impact on sensitivity to ATP-competitive and allosteric ABL1 inhibitors. *Leukemia* **31**, 1096–1107 (2017). doi:10.1038/leu.2016.353 Medline
72. C. Greenman, P. Stephens, R. Smith, G. L. Dalgliesh, C. Hunter, G. Bignell, H. Davies, J. Teague, A. Butler, C. Stevens, S. Edkins, S. O'Meara, I. Vastrik, E. E. Schmidt, T. Avis, S. Barthorpe, G. Bhamra, G. Buck, B. Choudhury, J. Clements, J. Cole, E. Dicks, S. Forbes, K. Gray, K. Halliday, R. Harrison, K. Hills, J. Hinton, A. Jenkinson, D. Jones, A. Menzies, T. Mironenko, J. Perry, K. Raine, D. Richardson, R. Shepherd, A. Small, C. Tofts, J. Varian, T. Webb, S. West, S. Widaa, A. Yates, D. P. Cahill, D. N. Louis, P. Goldstraw, A. G. Nicholson, F. Brasseur, L. Looijenga, B. L. Weber, Y. E. Chiew, A. DeFazio, M. F. Greaves, A. R. Green, P. Campbell, E. Birney, D. F. Easton, G. Chenevix-Trench, M. H. Tan, S. K. Khoo, B. T. Teh, S. T. Yuen, S. Y. Leung, R. Wooster, P. A. Futreal, M. R. Stratton, Patterns of somatic mutation in human cancer genomes. *Nature* **446**, 153–158 (2007). doi:10.1038/nature05610 Medline
73. J. A. Adams, Kinetic and catalytic mechanisms of protein kinases. *Chem. Rev.* **101**, 2271–2290 (2001). doi:10.1021/cr000230w Medline
74. N. Kannan, A. F. Neuwald, Did protein kinase regulatory mechanisms evolve through elaboration of a simple structural component? *J. Mol. Biol.* **351**, 956–972 (2005). doi:10.1016/j.jmb.2005.06.057 Medline
75. M. Bukhtiyarova, M. Karpusas, K. Northrop, H. V. M. Namboodiri, E. B. Springman, Mutagenesis of p38α MAP kinase establishes key roles of Phe169 in function and structural dynamics and reveals a novel DFG-OUT state. *Biochemistry* **46**, 5687–5696 (2007). doi:10.1021/bi0622221 Medline
76. S. H. Schmidt, M. J. Knape, D. Boassa, N. Mumdey, A. P. Kornev, M. H. Ellisman, S. S. Taylor, F. W. Herberg, The dynamic switch mechanism that leads to activation of LRRK2 is embedded in the DFGψ motif in the kinase domain. *Proc. Natl. Acad. Sci. U.S.A.* **116**, 14979–14988 (2019). doi:10.1073/pnas.1900289116 Medline
77. T. Saleh, P. Rossi, C. G. Kalodimos, Atomic view of the energy landscape in the allosteric regulation of Abl kinase. *Nat. Struct. Mol. Biol.* **24**, 893–901 (2017). doi:10.1038/nsmb.3470 Medline
78. J. Zhang, F. J. Adrián, W. Jahnke, S. W. Cowan-Jacob, A. G. Li, R. E. Iacob, T. Sim, J. Powers, C. Dierks, F. Sun, G.-R. Guo, Q. Ding, B. Okram, Y. Choi, A. Wojciechowski, X. Deng, G. Liu, G. Fendrich, A. Strauss, N. Vajpai, S. Grzesiek, T.

Tuntland, Y. Liu, B. Bursulaya, M. Azam, P. W. Manley, J. R. Engen, G. Q. Daley, M. Warmuth, N. S. Gray, Targeting Bcr-Abl by combining allosteric with ATP-binding-site inhibitors. *Nature* **463**, 501–506 (2010). doi:10.1038/nature08675 Medline
79. A. A. Wylie, J. Schoepfer, W. Jahnke, S. W. Cowan-Jacob, A. Loo, P. Furet, A. L. Marzinzik, X. Pelle, J. Donovan, W. Zhu, S. Buonamici, A. Q. Hassan, F. Lombardo, V. Iyer, M. Palmer, G. Berellini, S. Dodd, S. Thohan, H. Bitter, S. Branford, D. M. Ross, T. P. Hughes, L. Petruzzelli, K. G. Vanasse, M. Warmuth, F. Hofmann, N. J. Keen, W. R. Sellers, The allosteric inhibitor ABL001 enables dual targeting of BCR-ABL1. *Nature* **543**, 733–737 (2017). doi:10.1038/nature21702 Medline
80. F. E. Kwarcinski, K. R. Brandvold, S. Phadke, O. M. Beleh, T. K. Johnson, J. L. Meagher, M. A. Seeliger, J. A. Stuckey, M. B. Soellner, Conformation-selective analogues of dasatinib reveal insight into kinase inhibitor binding and selectivity. *ACS Chem. Biol.* **11**, 1296–1304 (2016). doi:10.1021/acschembio.5b01018 Medline
81. B. Nagar, O. Hantschel, M. Seeliger, J. M. Davies, W. I. Weis, G. Superti-Furga, J. Kuriyan, Organization of the SH3-SH2 unit in active and inactive forms of the c-Abl tyrosine kinase. *Mol. Cell* **21**, 787–798 (2006). doi:10.1016/j.molcel.2006.01.035 Medline
82. P. Filippakopoulos, M. Kofler, O. Hantschel, G. D. Gish, F. Grebien, E. Salah, P. Neudecker, L. E. Kay, B. E. Turk, G. Superti-Furga, T. Pawson, S. Knapp, Structural coupling of SH2-kinase domains links Fes and Abl substrate recognition and kinase activation. *Cell* **134**, 793–803 (2008). doi:10.1016/j.cell.2008.07.047 Medline
83. S. Lorenz, P. Deng, O. Hantschel, G. Superti-Furga, J. Kuriyan, Crystal structure of an SH2-kinase construct of c-Abl and effect of the SH2 domain on kinase activity. *Biochem. J.* **468**, 283–291 (2015). doi:10.1042/BJ20141492 Medline
84. F. Grebien, O. Hantschel, J. Wojcik, I. Kaupe, B. Kovacic, A. M. Wyrzucki, G. D. Gish, S. Cerny-Reiterer, A. Koide, H. Beug, T. Pawson, P. Valent, S. Koide, G. Superti-Furga, Targeting the SH2-kinase interface in Bcr-Abl inhibits leukemogenesis. *Cell* **147**, 306–319 (2011). doi:10.1016/j.cell.2011.08.046 Medline
85. B. H. Honig, W. L. Hubbell, Stability of "salt bridges" in membrane proteins. *Proc. Natl. Acad. Sci. U.S.A.* **81**, 5412–5416 (1984). doi:10.1073/pnas.81.17.5412 Medline
86. Y. Shan, M. A. Seeliger, M. P. Eastwood, F. Frank, H. Xu, M. Ø. Jensen, R. O. Dror, J. Kuriyan, D. E. Shaw, A conserved protonation-dependent switch controls drug binding in the Abl kinase. *Proc. Natl. Acad. Sci. U.S.A.* **106**, 139–144 (2009). doi:10.1073/pnas.0811223106 Medline
87. Y. Meng, Y. L. Lin, B. Roux, Computational study of the "DFG-flip" conformational transition in c-Abl and c-Src tyrosine kinases. *J. Phys. Chem. B* **119**, 1443–1456 (2015). doi:10.1021/jp511792a Medline
88. S. R. Hubbard, L. Wei, W. A. Hendrickson, Crystal structure of the tyrosine kinase domain of the human insulin receptor. *Nature* **372**, 746–754 (1994). doi:10.1038/372746a0 Medline
89. M. A. Lemmon, J. Schlessinger, Cell signaling by receptor tyrosine kinases. *Cell* **141**, 1117–1134 (2010). doi:10.1016/j.cell.2010.06.011 Medline
90. W. Jankowski, T. Saleh, M.-T. Pai, G. Sriram, R. B. Birge, C. G. Kalodimos, Domain organization differences explain Bcr-Abl's preference for CrkL over CrkII. *Nat. Chem. Biol.* **8**, 590–596 (2012). doi:10.1038/nchembio.954 Medline
91. P. Rossi, Y. R. Monneau, Y. Xia, Y. Ishida, C. G. Kalodimos, Toolkit for NMR studies of methyl-labeled proteins. *Methods Enzymol.* **614**, 107–142 (2019). doi:10.1016/bs.mie.2018.08.036 Medline
92. Y. R. Monneau, Y. Ishida, P. Rossi, T. Saio, S. R. Tzeng, M. Inouye, C. G. Kalodimos, Exploiting *E. coli* auxotrophs for leucine, valine, and threonine specific methyl labeling of large proteins for NMR applications. *J. Biomol. NMR* **65**, 99–108 (2016). doi:10.1007/s10858-016-0041-1 Medline
93. F. Delaglio, S. Grzesiek, G. W. Vuister, G. Zhu, J. Pfeifer, A. Bax, NMRPipe: A multidimensional spectral processing system based on UNIX pipes. *J. Biomol. NMR* **6**, 277–293 (1995). doi:10.1007/BF00197809 Medline
94. W. Lee, M. Tonelli, J. L. Markley, NMRFAM-SPARKY: Enhanced software for biomolecular NMR spectroscopy. *Bioinformatics* **31**, 1325–1327 (2015). doi:10.1093/bioinformatics/btu830 Medline
95. P. Rossi, Y. Xia, N. Khanra, G. Veglia, C. G. Kalodimos, ^{15}N and ^{13}C- SOFAST-HMQC editing enhances 3D-NOESY sensitivity in highly deuterated, selectively [^{1}H,^{13}C]-labeled proteins. *J. Biomol. NMR* **66**, 259–271 (2016). doi:10.1007/s10858-016-0074-5 Medline
96. Y. R. Monneau, P. Rossi, A. Bhaumik, C. Huang, Y. Jiang, T. Saleh, T. Xie, Q. Xing, C. G. Kalodimos, Automatic methyl assignment in large proteins by the MAGIC algorithm. *J. Biomol. NMR* **69**, 215–227 (2017). doi:10.1007/s10858-017-0149-y Medline
97. P. Vallurupalli, G. Bouvignies, L. E. Kay, Studying "invisible" excited protein states in slow exchange with a major state conformation. *J. Am. Chem. Soc.* **134**, 8148–8161 (2012). doi:10.1021/ja3001419 Medline
98. O. F. Lange, P. Rossi, N. G. Sgourakis, Y. Song, H. W. Lee, J. M. Aramini, A. Ertekin, R. Xiao, T. B. Acton, G. T. Montelione, D. Baker, Determination of solution structures of proteins up to 40 kDa using CS-Rosetta with sparse NMR data from deuterated samples. *Proc. Natl. Acad. Sci. U.S.A.* **109**, 10873–10878 (2012). doi:10.1073/pnas.1203013109 Medline
99. P. Güntert, L. Buchner, Combined automated NOE assignment and structure calculation with CYANA. *J. Biomol. NMR* **62**, 453–471 (2015). doi:10.1007/s10858-015-9924-9 Medline
100. A. T. Brunger, Version 1.2 of the Crystallography and NMR system. *Nat. Protoc.* **2**, 2728–2733 (2007). doi:10.1038/nprot.2007.406 Medline

ACKNOWLEDGMENTS

We wish to thank Z. Xia for help with molecular cloning, Y. Xia for help with the NMR experiments, Z. Luo for producing the animations, G. Bouvignies for providing the ChemEx software, L. Kay and R. Anderson for discussions, and B. Young for the synthesis of the labeled Phe and Tyr. NMR spectra were acquired at the St. Jude Biomolecular NMR Spectroscopy Center. **Funding:** This work was supported by the U.S. National Institutes of Health grant R35 GM122462 (C.G.K.) and ALSAC. **Author contributions:** T.X. and C.G.K. conceived the study and designed the experimental approach. T.X. prepared all protein samples, determined the Abl structures, and performed the activity assays. T.S. assisted with the kinase assays and P.R. assisted with the structure determination. T.X. and C.G.K. wrote the manuscript. **Competing interests:** The authors declare no competing interests. **Data and materials availability:** Atomic coordinates and NMR chemical shifts have been deposited in the Protein data Bank (PDB) and Biological Magnetic Resonance Data Bank (BMRB), respectively, under the following accession codes: 6XR6 and 30770 for the active state of Abl, 6XR7 and 30771 for the inactive state 1 (I_1) of Abl, and 6XRG and 30772 for the inactive state 2 (I_2) of Abl. All other data are available in the main text or the supplementary materials. Requests for materials should be addressed to the corresponding author.

SUPPLEMENTARY MATERIALS

science.sciencemag.org/cgi/content/full/science.abc2754/DC1
Figs. S1 to S12
Table S1
References
MDAR Reproducibility Checklist
Movies S1 to S3

16 April 2020; accepted 12 August 2020
Published online 1 October 2020
10.1126/science.abc2754

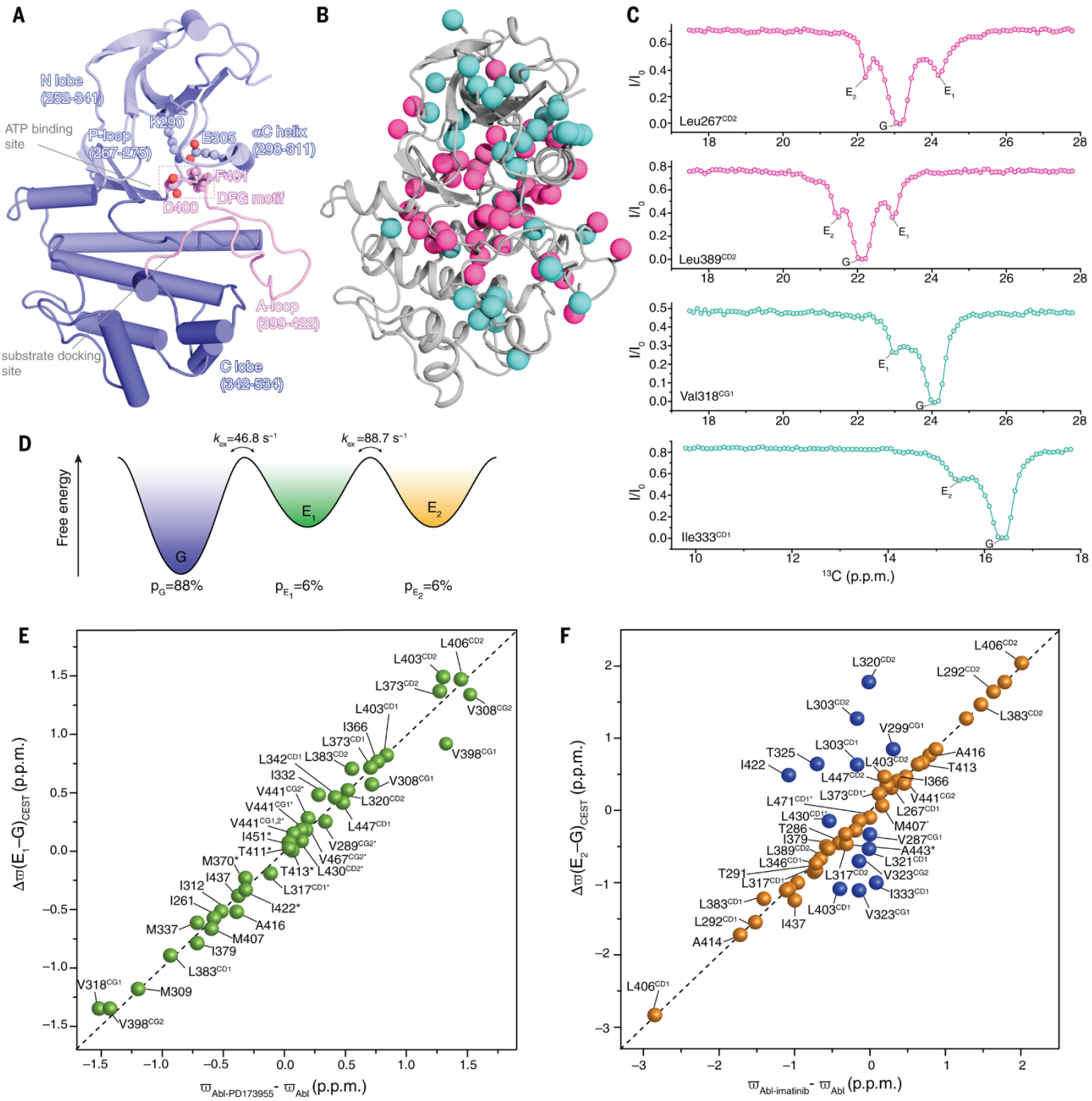

Fig. 1. Characterization of the energetically excited conformational states in Abl kinase by NMR CEST experiments. (**A**) Structure of the Abl kinase domain in the active conformation determined in the current work. Key structural features are highlighted. (**B**) Methyl groups in Abl indicating the presence of one (colored cyan) or two (colored magenta) excited conformational states in the NMR CEST experiments. (**C**) Representative ^{13}C CEST profiles of the indicated methyl groups. The major dip corresponds to the major (ground) state whereas the minor dips correspond to the energetically excited conformational states E_1 and E_2. As explained in the main text, excited states E_1 and E_2 correspond to inactive states I_1 and I_2, respectively. (**D**) Energy landscape of the ground (G), E_1 and E_2 states denoting their populations and kinetics of interconversion as measured by fitting the CEST data. (**E**) Correlation of the CEST-derived chemical shift difference between the ground and E_1 states $[\Delta\varpi(E_1–G)_{CEST}]$ with the chemical shift difference between apo and PD173955-bound Abl. Methyls (marked with an asterisk) for which the dips corresponding to the ground and E_1 states are within ±0.3 p.p.m. cannot be resolved in the CEST profile and their chemical shift difference was extracted from ^{1}H-^{13}C–correlated experiments (see Materials and methods). Methyls that are close (within 6 Å) to PD173955 were excluded from the correlation because their chemical shifts are directly affected by the inhibitor. $Val398^{CG1}$ deviates from linearity because of the rearrangement of the nearby Phe401 side chain in the inhibitor complex compared to the E_1 state. (**F**) Correlation of the CEST-derived chemical shift difference between the ground and E_2 states $[\Delta\varpi(E_2–G)_{CEST}]$ with the chemical shift difference between apo and imatinib-bound Abl. Methyls that are close (within 6 Å) to imatinib were excluded from the correlation because their chemical shifts are directly affected by the inhibitor. Methyls colored blue deviate from linearity as discussed in the text and in fig. S8. Methyls (marked with an asterisk) for which the dips corresponding to the ground and E_2 states are within ±0.3 p.p.m. cannot be resolved in the CEST profile and their chemical shift difference was extracted from ^{1}H-^{13}C–correlated experiments.

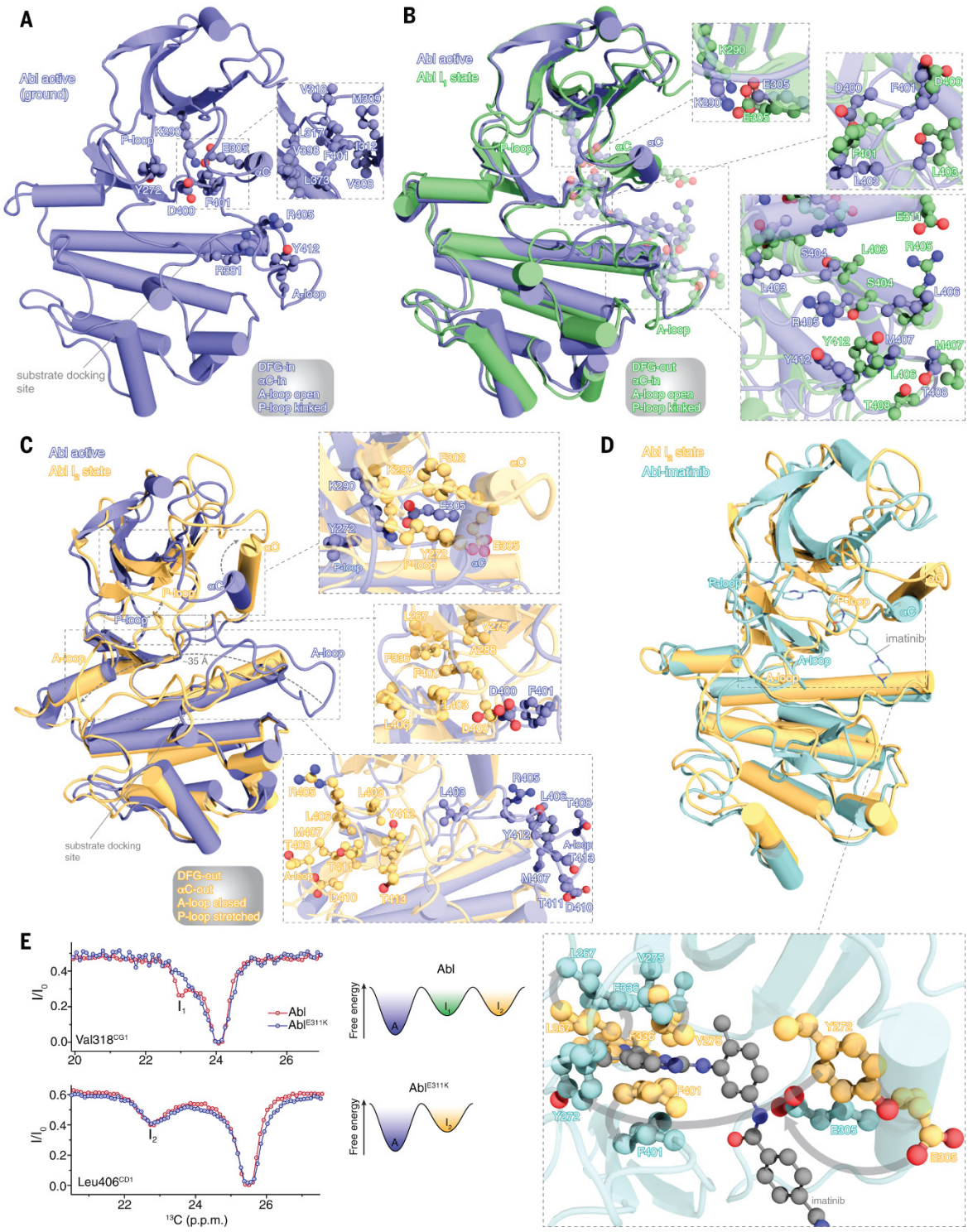

Fig. 2. Structures of the ground (active), E_1 (I_1) and E_2 (I_2) states of Abl. (**A**) NMR solution structure of the ground state of Abl shows that the Abl kinase domain inherently adopts the fully active state. The zoomed view shows the hydrophobic residues surrounding Phe401. (**B**) Structure of the Abl E_1 state (green) superimposed on the structure of the active state (blue). Because Abl E_1 adopts an inactive state is referred to as I_1. The zoomed views highlight similarities (e.g., αC helix) and differences (e.g., DFG motif and A-loop) in the disposition of key structural elements between the two states. (**C**) Structure of the Abl E_2 state (orange) superimposed on the structure of the active state (blue). Because Abl E_2 adopts an inactive state is referred to as I_2. The major structural rearrangement undergone by the αC helix, the A-loop and the P-loop between the two states is indicated by an arrow. (**D**) Superposition of the structures of the Abl I_2 state (orange) and the Abl–imatinib complex (cyan; PDB ID 1IEP). The zoomed view highlights the structural rearrangement upon imatinib binding in the residues lining the pocket. (**E**) ^{13}C CEST profiles of Abl and Abl^{E311K} demonstrate that the E311K substitution destabilizes the Abl I_1 state but has no apparent effect on the I_2 state. A denotes active state. The E311K substitution abrogates the ion pair between Glu311 and Arg405 in the I_1 state (B).

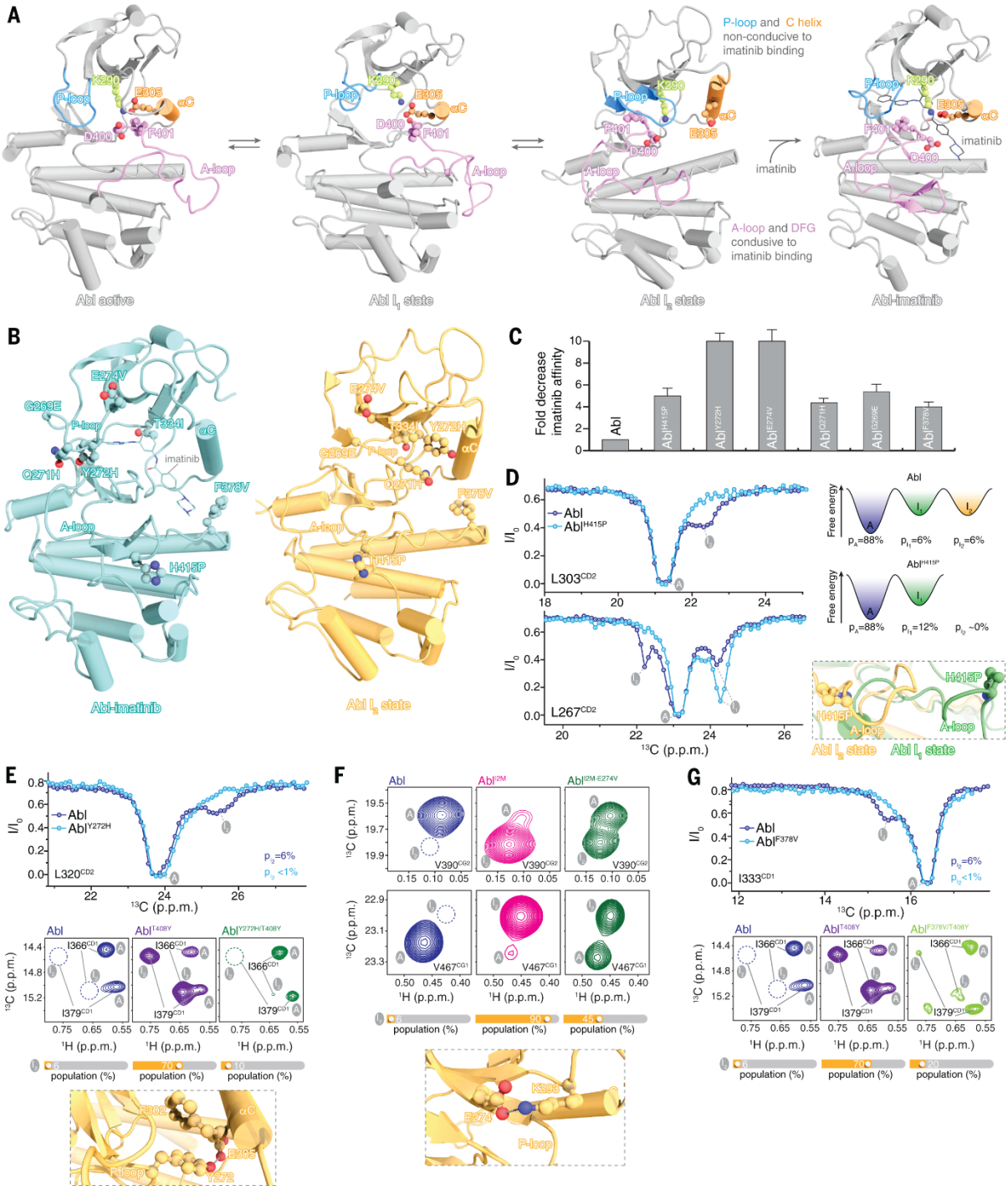

Fig. 3. Structural and energetic dissection of imatinib-resistance Abl variants. (**A**) Structures of the three Abl conformational states and binding of imatinib to the I_2 state highlighting the disposition of key structural elements. (**B**) Patient-derived imatinib-resistance mutants studied here shown on the structure of Abl in complex with imatinib and on the structure of the Abl I_2 state. (**C**) Change in affinity for imatinib by the Abl variants relative to wild type Abl as determined by ITC (fig. S9). Error bars are standard deviation determined from a triplicate. (**D**) Effect of the H415P substitution on the population of the Abl states measured by ^{13}C CEST experiments. The changes in the populations are indicated in a free energy diagram. A zoomed view of the mutation site suggests how the Pro substitution may destabilize the Abl I_2 state. (**E**) Effect of the Y272H substitution on the population of the Abl states measured by ^{13}C CEST using the wild type Abl as reference (top) and by ^{1}H-^{13}C–correlated experiments using the Abl^{T408Y} variant, which populates Abl I_2 state at 70%, as reference (bottom). A zoomed view of the mutation site indicates that substitution of Tyr272 will disrupt the hydrogen bond to Glu305 thereby destabilizing the Abl I_2 state. (**F**) Effect of the E274V substitution on the population of the Abl states measured by ^{1}H-^{13}C–correlated spectra using the Abl^{I2M} variant as reference. A zoomed view of the mutation site indicates that substitution of Glu274 will disrupt the hydrogen bond to Lys293 thereby destabilizing the Abl I_2 state. (**G**) Effect of the F378V substitution on the population of the Abl states measured by ^{13}C CEST using the wild type Abl as reference (top) and by ^{1}H-^{13}C–correlated spectra using the Abl^{T408Y} variant as reference (bottom). For additional data and discussion see fig. S10.

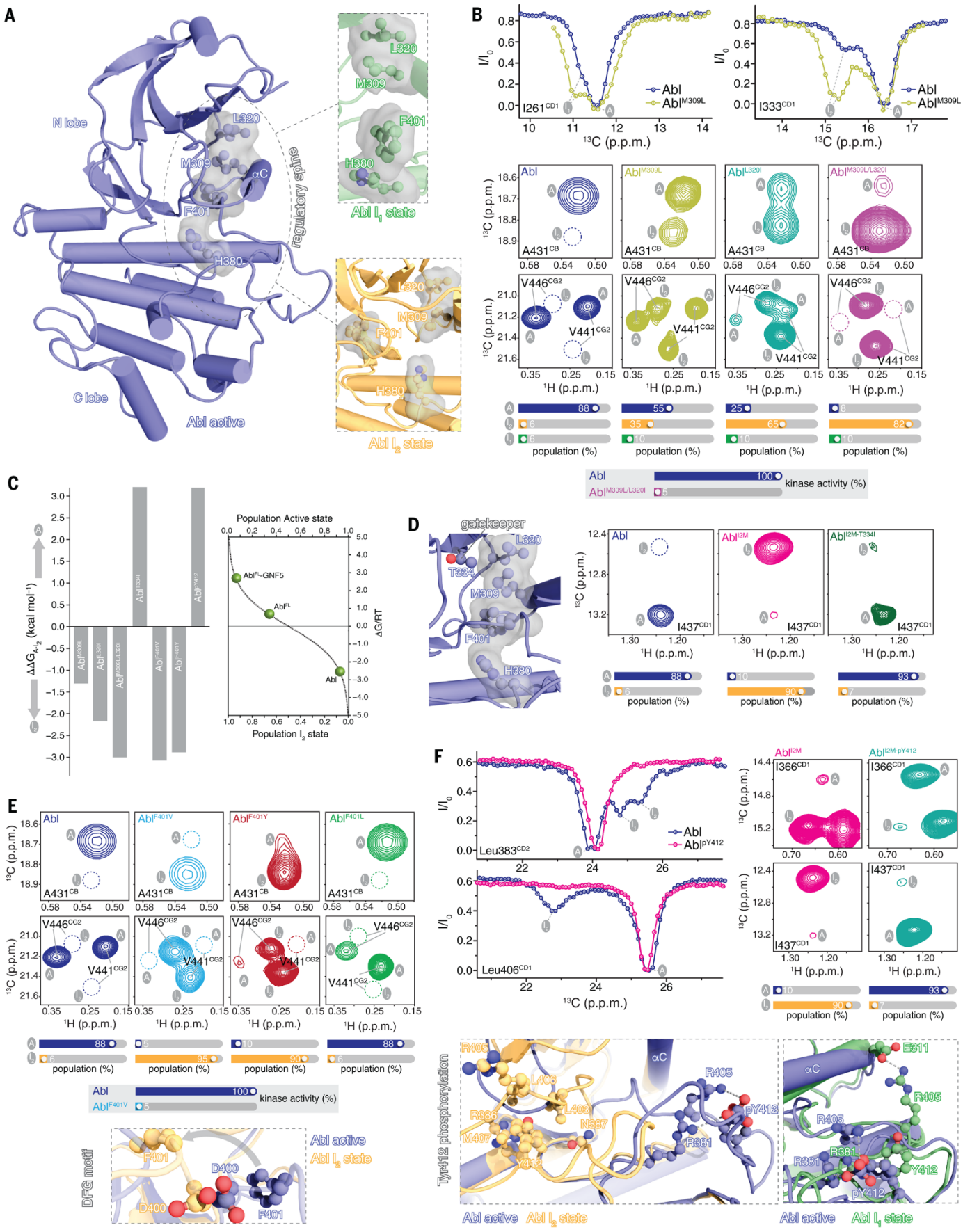

Fig. 4. Quantitative dissection of the effect of the regulatory spine, the gatekeeper, the DFG motif, and phosphorylation on the Abl conformational ensemble. (**A**) Structure of the active state of Abl highlighting the regulatory spine, made up by Met309, Leu320, His380, and Phe401. The disposition of the regulatory spine is also shown for Abl states I_1 and I_2. (**B**) Effect of amino acid substitutions at the regulatory spine on the populations of the Abl conformational states as measured by NMR. Because the k_{ex} rates of the transitions (Fig. 1D) are slow on the NMR chemical shift time scale the resonances of the individual conformational states can be seen in ^{1}H-^{13}C–correlated spectra if their population is above ~5%. Thus, in addition to ^{13}C CEST, ^{1}H-^{13}C–correlated experiments were also used to quantitate the populations, especially for Abl variants that are not stable over the period of time required for CEST experiments (Materials and methods). There is excellent agreement in the population measurements by CEST and ^{1}H-^{13}C–correlated experiments. The labeling scheme of the Abl variants is as shown in fig. S1. Determination of the kinase activity (fig. S11) shows that the $Abl^{M309L/L320I}$ variant inhibits Abl. (**C**) Energy contribution to the active and I_2 states of Abl by the indicated variants. Negative values of ΔΔG indicate increased stability of the Abl I_2 state whereas positive values indicate increased stability of the Abl active state. A graph is included where the populations of the active and I_2 states are plotted as a function of the associated free energy, ΔG/RT, where R is the gas constant and T is the temperature. A 0.6 kcal mol^{-1} change in ΔG corresponds to a change by 1 unit in ΔG/RT at room temperature (*77*). The populations of the two states for Abl (isolated kinase domain) and full-kinase Abl^{FK} are shown to help assess the effect that each one of the variants has on the activation or inhibition of Abl. (**D**) Effect of the Thr334 to Ile substitution at the gatekeeper position on the populations of the Abl states. Given that Abl exists predominantly in the active state (p_A ~88%), to measure the full effect we used the Abl^{I2M} variant ($Abl^{G269E/M309L/T408Y}$), which populates predominantly the I_2 state (p_{I2} ~90%). (**E**) Effect of amino acid substitutions of the Phe residue in the DFG motif on the populations of the Abl states. Val or Tyr substitution results in an Abl kinase that adopts primarily the I_2 state. The low kinase activity of Abl^{F401V} is consistent with the NMR findings. (**F**) Effect of Tyr412 phosphorylation in the A-loop on the populations of the Abl states. Tyr412 phosphorylation eliminates both I_1 and I_2 states and stabilizes the active state as evidenced by ^{13}C CEST experiments. To measure the full effect, we used the Abl^{I2M} variant as discussed in (D). The zoomed views of the superposition of the structure of each of the inactive states on the structure of the active state provides mechanistic insight into the effect.

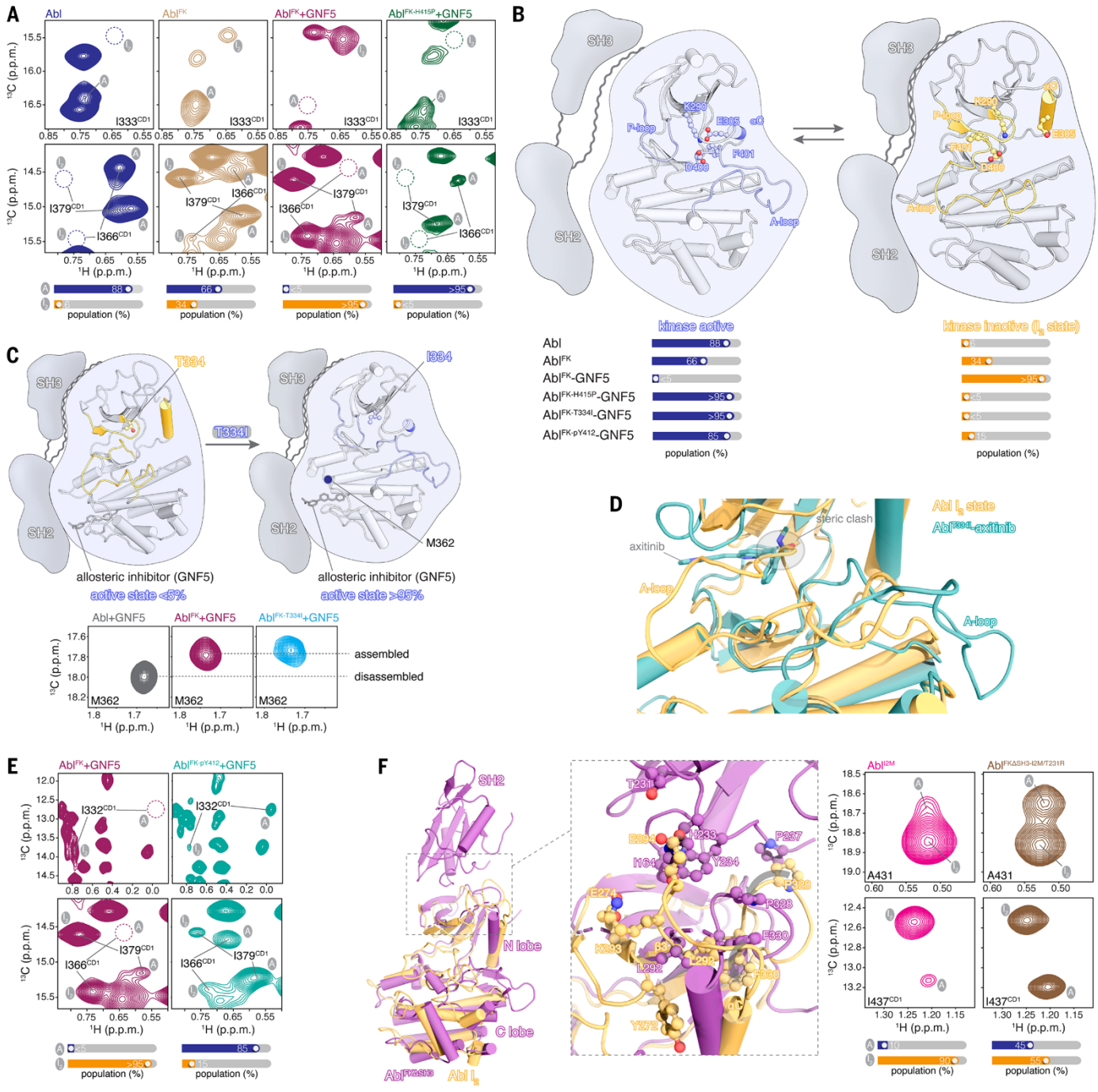

Fig. 5. Quantitative dissection of the effect of variants on the conformational ensemble of the full-length Abl kinase. (**A**) Effect of the SH3-SH2 regulatory module, the addition of the allosteric inhibitor GNF5, and the H415P substitution as measured by NMR. Abl^{FK} corresponds to the SH3-SH2-KD Abl fragment. Because Abl^{FK} is not sufficiently stable for ^{13}C CEST experiments, we used ^{1}H-^{13}C–correlated spectra to quantitate the populations. For the isolated Abl kinase domain we know from CEST experiments that the population of the I_1 state is 6%. However, while we can conclude from the ^{1}H-^{13}C–correlated spectra that the population of the I_1 state does not increase in Abl^{FK} and its variants, we cannot conclude if it is depleted. Thus, the populations reported for Abl^{FK} variants are only for the active and the I_2 states. (**B**) Schematic of Abl^{FK} showing the equilibrium between a disassembled conformation, wherein the regulatory module is not bound to the kinase domain, and an assembled conformation, wherein the regulatory module is docked onto the back of the kinase domain. In the disassembled conformation the kinase adopts the active state whereas in the assembled one it adopts the I_2 state. The populations of the active and I_2 states in the Abl variants studied are indicated. (**C**) Schematic of Abl^{FK} summarizing the effect of the gatekeeper T334I substitution, which forces Abl to adopt the active state even when the regulatory module is docked onto the kinase. ^{1}H-^{13}C–correlated spectra showing the M362 methyl resonance. M362 is located at the interface between the SH2 and the kinase domain and provides a sensitive probe for the assembled conformation. (**D**) Superposition of the structures of the Abl I_2 state and the Abl^{T334I}–axitinib complex (PDB ID 4TWP) highlights the steric clash between the bound inhibitor and the A-loop in the I_2 state, which explains the higher affinity of the inhibitor for the T334I variant. (**E**) Effect of Tyr412 phosphorylation on the populations of the active and I_2 states of Abl^{FK} in complex with the allosteric inhibitor GNF5 measured by NMR. (**F**) Effect of the extended conformation, wherein the SH2 domain docks on the top of the N-lobe, on the populations of the active and I_2 states of Abl measured by NMR. The structure of the $Abl^{FK\Delta SH3}$ fragment (purple; PDB ID 4XEY) is superimposed on the structure of the Abl I_2 state (orange).

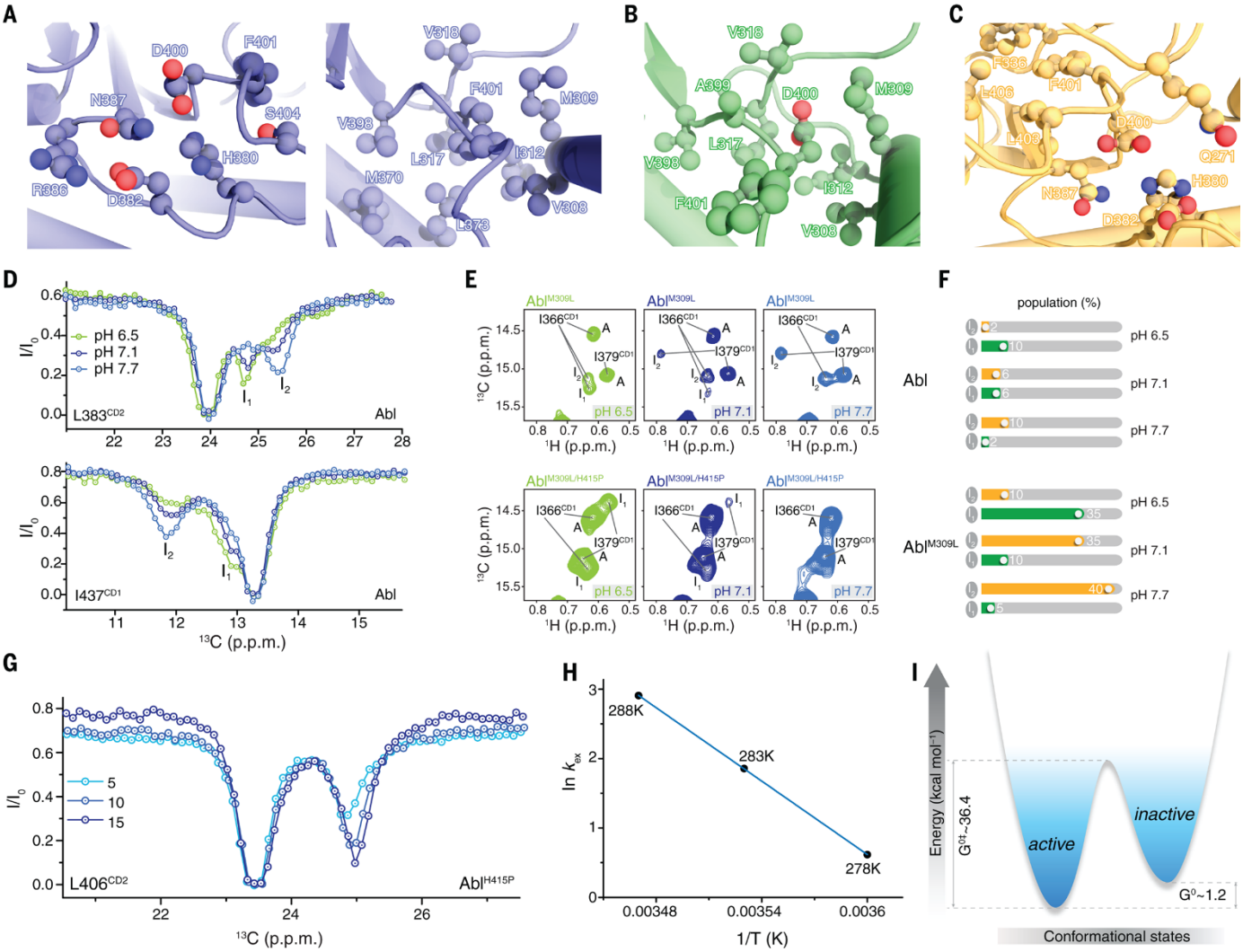

Fig. 6. pH effect on the Abl conformational ensemble and activation energy of the DFG transition. (**A** to **C**) Close-up view of the DFG motif conformation in the (A) active state, (B) the I_1 state and (C) the I_2 state. The positioning of Asp400 of the DFG motif differs among the various conformational states. In the active state Asp400 is exposed to the solvent whereas Phe401 is buried inside a hydrophobic pocket. The DFG motif flips 180° as it transitions from the active to the I_1 state with the two residues swapping positions: in the I_1 state Asp400 is now positioned inside the hydrophobic pocket while Phe401 is exposed to the solvent. Although the DFG motif remains in the *"out"* conformation in the I_2 state, the A-loop undergoes a major rearrangement and as a result Asp400 is found in a polar environment, similarly to the active state, and Phe401 is buried inside the hydrophobic pocket located in the nucleotide binding site. (**D**) ^{13}C CEST profiles of representative residues as a function of pH. The results show that lower pH (pH 6.5) stabilizes selectively the I_1 state while higher pH (pH 7.7) stabilizes selectively the I_2 state. (**E**) ^{1}H-^{13}C–correlated spectra of Abl^{M309L} and $Abl^{M309L/H415P}$ variants as a function of pH. In $Abl^{M309L/H415P}$ at pH 7.7 there is no detectable inactive state because the H415P substitution eliminates the I_2 state and the higher pH depletes the I_1 state. (**F**) Populations of the I_1 and I_2 states as a function of pH. The relative populations of the I_1 and I_2 states fluctuate antagonistically but the ratio of populations between the active state and the inactive states collectively is not affected by changes in pH within this range. (**G**) ^{13}C CEST profiles of Abl^{H415P} as a function of temperature. (**H**) Arrhenius plot of the k_{ex} measured by the CEST experiments in (G) for the three temperatures indicated used to determine the activation energy of the DFG transition from the active to the I_1 inactive conformation. (**I**) Energy diagram indicating the activation enthalpy (~36.4 kcal mol^{-1}) of the DFG flip from DFG-*in* to DFG-*out*.

Conformational states dynamically populated by a kinase determine its function

Tao Xie, Tamjeed Saleh, Paolo Rossi and Charalampos G. Kalodimos

published online October 1, 2020

Science (print ISSN 0036-8075; online ISSN 1095-9203) is published by the American Association for the Advancement of Science, 1200 New York Avenue NW, Washington, DC 20005. The title *Science* is a registered trademark of AAAS.